CoCliCo

Research and Innovation Action (RIA)

This project has received funding from the European Union's Horizon 2020 research and innovation programme under grant agreement No 101003598

Start date : 2021-09-01 Duration : 48 Months

High-resolution relative mean sea-level hindcast and projections

Authors : Dr. Gianmaria SANNINO (ENEA), Angélique Melet (Mercator), Alessandro Anav (ENEA), Maialen Irazoqui (Mercator), Adriana Carillo (ENEA), Roberto Iacono (ENEA), Guillaume Reffray (Mercator)

CoCliCo - Contract Number: 101003598

Project officer: Anna Natasa ASIK

Document title	High-resolution relative mean sea-level hindcast and projections
Author(s)	Dr. Gianmaria SANNINO, Angélique Melet (Mercator), Alessandro Anav (ENEA), Maialen Irazoqui (Mercator), Adriana Carillo (ENEA), Roberto Iacono (ENEA), Guillaume Reffray (Mercator)
Number of pages	50
Document type	Deliverable
Work Package	WP3
Document number	D3.3
Issued by	ENEA
Date of completion	2025-03-20 11:10:43
Dissemination level	Public

Summary

The CoCliCo project addresses the critical need for accurate, high-resolution projections of coastal sea-level changes to support adaptation planning and risk mitigation. The document presents significant advancements in regional climate modeling, focusing on the Mediterranean and European continental shelf regions. By employing state-of-the-art dynamical downscaling techniques, the project delivers refined projections of sea-level dynamics and associated climatic variables under different emission scenarios.

Approval

Date	By
2025-03-21 13:42:26	Mrs. Melisa MENENDEZ (UC)
2025-03-24 11:06:25	Dr. Gonéri LE COZANNET (BRGM)

CoCliCo
coastal climate core services

D3.3 High-resolution relative mean sea-level hindcast and projections'

Release Status: DRAFT

Dissemination level: Confidential Consortium & EU Commission

Author: Gianmaria Sannino, Angélique Melet, Alessandro Anav, Maialen Irazoqui, Adriana Carillo, Roberto Iacono, Guillaume Reffray

Date: 19/03/2025

Filename and version:

Project ID NUMBER 101003598

Call: H2020-LC-CLA-2020-2

DG/Agency: European Climate Infrastructure and Environment Executive Agency (CINEA)

This project has received funding from the European Union's Horizon 2020 research and innovation programme under grant agreement No. 101003598

CoCliCo
coastal climate core services

Document History

Revision History

This document has been through the following revisions:

Version No.	Revision Date	Filename/Location stored:	Brief Summary of Changes
1	13 February 2025		

Distribution

This document has been distributed to:

Name	Title	Version Issued	Date of Issue
			00/00/0000

This project has received funding from the European Union's Horizon 2020 research and innovation programme under grant agreement No. 101003598

Disclaimer

The information and views set out in this report are those of the author(s) and do not necessarily reflect the official opinion of the European Union. Neither the European Union institutions and bodies nor any person acting on their behalf may be held responsible for the use which may be made of the information contained therein.

This project has received funding from the European Union's Horizon 2020 research and innovation programme under grant agreement No. 101003598

Executive summary

The CoCliCo project addresses the critical need for accurate, high-resolution projections of coastal sea-level changes to support adaptation planning and risk mitigation. The document presents significant advancements in regional climate modeling, focusing on the Mediterranean and European continental shelf regions. By employing state-of-the-art dynamical downscaling techniques, the project delivers refined projections of sea-level dynamics and associated climatic variables under different emission scenarios.

This project has received funding from the European Union's Horizon 2020 research and innovation programme under grant agreement No. 101003598

Table of Contents

This project has received funding from the European Union's Horizon 2020 research and innovation programme under grant agreement No. 101003598

1. Introduction

Sea level (SL) changes at the coast are influenced by an interplay of global, regional, and local factors. On a global scale, the primary driver of SL change is the rise in global mean sea level (GMSL), resulting from the thermal expansion of seawater and the transfer of mass from land-based liquid /solid water reservoirs, including glaciers and ice sheets, into the ocean (Church et al., 2013; Slangen et al., 2017). At regional scales, spatial variations in SL changes occur due to ocean dynamic processes, such as shifts in ocean circulation and the redistribution of heat, salt, and mass (Forget and Ponte, 2015; Meyssignac et al., 2017), as well as to changes in Earth's gravity, rotation and deformation (GRD effects, Gregory et al., 2019) associated to land ice mass loss. At the local level, additional factors—such as tidal fluctuations, wind-driven surges, and variations in atmospheric pressure—further modulate SL changes, often amplifying deviations from the GMSL (Melet et al., 2018; Woodworth et al., 2019). These deviations are particularly pronounced along coastlines, where complex interactions between oceanic and atmospheric processes are more prevalent.

Global climate models (GCMs) are the primary tools for producing long-term SL projections under different socio-economic and associated greenhouse gases emission scenarios (Fox-Kemper et al., 2021; Oppenheimer et al., 2019; Church et al., 2013; Slangen et al., 2014). However, the spatial resolution of GCMs, typically on the order of 1° (approximately 100 km at mid-latitudes) in the ocean, is insufficient to capture the mesoscale and fine-scale processes that strongly influence coastal SL dynamics (Woodworth et al., 2019). This limitation introduces significant biases in coastal SL projections, particularly in regions dominated by local processes such as tidal interactions and atmospheric forcing. For instance, studies in the Caribbean and North Pacific have reported discrepancies of up to 15 cm between SL projections derived from coarse-resolution GCMs and those generated using higher-resolution regional models (Liu et al., 2016; Zhang et al., 2017; Jin et al., 2021), underscoring the need for improved methodologies.

Dynamical downscaling has emerged as a robust approach to address these limitations. By employing high-resolution regional climate models (RCMs) forced with outputs from GCMs, this method explicitly incorporates processes such as tides, atmospheric pressure effects, and localized wind-driven circulation (Adloff et al., 2018; Hermans et al., 2020b). Dynamical downscaling not only enhances the spatial resolution of SL projections but also captures the intricate interplay of physical processes at regional and coastal scales. Previous studies have demonstrated the advantages of this approach, reporting significant improvements in the accuracy and detail of SL projections across diverse geographic regions (Macias et al., 2018; Gomis et al., 2016; Shin and Alexander, 2020).

This project has received funding from the European Union's Horizon 2020 research and innovation programme under grant agreement No. 101003598

The use of dynamical downscaling to refine spatial resolution and incorporate processes critical to coastal dynamics—such as tidal interactions and localized atmospheric forcing—represents a significant advancement in SL projection methodologies and supports user needs for more regional to local information (Jimenez et al., 2024; Melet et al., 2024; McInnes et al., 2024). In this deliverable, we present advanced regional models developed to produce climate data that will be integrated into the CoCliCo coastal climate platform.

It is important to emphasize that the research conducted as part of this project has already resulted in some scientific publications, which offer a detailed and comprehensive analysis of the findings. This deliverable focuses specifically only on the development of numerical models and key outcomes derived from their application. For a complete overview of the work conducted, readers are encouraged to consult the following published papers:

1) Anav, A., Antonelli, M., Calmanti, S. et al. Dynamical downscaling of CMIP6 scenarios with ENEA-REG: an impact-oriented application for the Med-CORDEX region. Clim Dyn 62, 3261–3287 (2024). https://doi.org/10.1007/s00382-023-07064-3
2) Cappucci, S.; Carillo, A.;Iacono, R.; Moretti, L.; Palma, M.;Righini, G.; Antonioli, F.; Sannino, G. Evolution of Coastal Environments under Inundation Scenarios Using an Oceanographic Model and Remote Sensing Data. Remote Sens. 2024, 16,2599. https://doi.org/10.3390/rs16142599
3) Chaigneau, A. A., Reffray, G., Voldoire, A., and Melet, A.: IBI-CCS: a regional high-resolution model to simulate sea level in western Europe, Geosci. Model Dev., 15, 2035–2062, https://doi.org/10.5194/gmd-15-2035-2022, 2022.
4) Chaigneau, A. A., Law-Chune, S., Melet, A., Voldoire, A., Reffray, G., and Aouf, L.: Impact of sea level changes on future wave conditions along the coasts of western Europe, Ocean Sci., 19, 1123–1143, https://doi.org/10.5194/os-19-1123-2023, 2023.
5) Chaigneau, A. A., Melet, A., Voldoire, A., Irazoqui Apecechea, M., Reffray, G., Law-Chune, S., and Aouf, L.: Dynamic projections of extreme sea levels for western Europe based on ocean and wind-wave modelling, Nat. Hazards Earth Syst. Sci., 24, 4031–4048, https://doi.org/10.5194/nhess-24-4031-2024, 2024.

2. High resolution mean sea-level change hindcasts and projections in the Med.

This project has received funding from the European Union's Horizon 2020 research and innovation programme under grant agreement No. 101003598

2.1. Model Description and Experimental Design

The ENEA-REG model (Anav et al., 2021) is a regional Earth System Model (ESM) designed for high-resolution climate studies. It integrates multiple modeling components, including atmosphere, ocean, land, and river routing. Data exchange, regridding, and interpolation between these components are facilitated by the RegESM coupler, as described in Turuncoglu (2019). RegESM is built upon the Earth System Modeling Framework (ESMF, version 7.1) and employs the National Unified Operational Prediction Capability (NUOPC) layer to ensure interconnectivity, synchronization, and horizontal grid interpolation.
ENEA-REG incorporates the Weather Research and Forecasting model (WRF, version 4.2.2; Skamarock and Klemp, 2008) for simulating atmospheric dynamics, the Massachusetts Institute of Technology General Circulation Model (MITgcm, version z67; Marshall et al., 1997) for oceanic state and circulation, and the Hydrological Discharge (HD, version 1.0.2; Hagemann and Dümenil, 1998; Hagemann and Gates, 2001) model for freshwater fluxes over land and river discharge to the ocean (Table 1).

Component	Details
Atmosphere	Model: WRF (v4.2.2) Domain: Med-CORDEX Horizontal resolution: 12 km Domain size: 480 × 350 cells (lon x lat) Vertical resolution: 50 hybrid levels up to 10 hPa Physical time step: 60 s Forcing: ERA5 (present) and MPI-ESM1-2-HR Relaxation zone: 10 points with an exponential relaxation Microphysics: Morrison (two–moment scheme) Cumulus parameterization: BMJ Shortwave radiation: RRTMG Longwave radiation: RRTMG Land-surface model: NOAH-MP Planetary boundary layer: YSU
Ocean	Model: MITgcm (z67) Domain: Mediterranean Sea Horizontal resolution: 1/12° Domain size: 570 × 264 cells (lon x lat) Vertical resolution: 75 z levels

This project has received funding from the European Union's Horizon 2020 research and innovation programme under grant agreement No. 101003598

	Time step: 150 s Forcing: ORAS5 (present) and MPI-ESM1-2-HR Relaxation zone: 18 grid points Vertical mixing: GGL90
Hydrology	Model: HD Resolution: 0.5° Time step: Daily
Driver	Name: RegESM Library: ESMF (v7.1)/NUOPC

Table 1. Setup of the ENEA-REG system along with the main physical parameterizations used in this study by the atmospheric and ocean components

Compared to Anav et al. (2021), this study incorporates several updates. The WRF model now employs hybrid vertical levels instead of sigma-p vertical coordinates and implements the double-moment microphysics and cumulus parameterizations of Morrison et al. (2009) and Janjić et al. (1994), respectively. The ocean model includes a full non-linear free-surface formulation (Campin et al., 2004). Ocean boundary conditions have been updated to include monthly sea-level fields, with temperature and salinity profiles prescribed as monthly means instead of climatological values. Spatially dependent horizontal viscosity is calculated using Leith's (1968) turbulence closure scheme, which resolves the direct enstrophy cascade characteristic of two-dimensional turbulence (Fox-Kemper and Menemenlis, 2008). A third-order direct space–time flux-limited scheme is used for tracer advection.

As in Anav et al. (2021), Nile and Black Sea conditions are prescribed as climatological monthly means, while the initial conditions for the starting month (August) are derived from hindcast simulations performed with the previous version of the ocean model, based on monthly climatological averages of temperature and salinity fields. Table 1 provides a summary of the main physical parameterizations used in this study for both atmospheric and oceanic components.

The atmospheric and oceanic models exchange sea surface temperature (SST), surface pressure, wind components, freshwater fluxes (evaporation–precipitation), and heat fluxes. Unlike the previous version, this study computes net heat flux as the sum of net longwave, net shortwave, latent heat, and sensible heat fluxes, while shortwave radiation is separately provided to allow for ocean penetration. The hydrological model calculates river discharge using surface and subsurface runoff data provided by WRF and exchanges this field with the ocean model to close the water cycle. Table 2 summarizes the fields exchanged among the model components. The coupling timestep between the atmosphere and ocean is set to 3 hours, while coupling with the hydrological model occurs daily.

This project has received funding from the European Union's Horizon 2020 research and innovation programme under grant agreement No. 101003598

Field	From	To
Sea surface temperature	MITgcm	WRF
Zonal wind	WRF	MITgcm
Meridional wind	WRF	MITgcm
Freshwater flux	WRF	MITgcm Given as evaporation minus precipitation
Solar heat flux	WRF	MITgcm Downward shortwave radiation considered as penetrative component of the air-sea heat flux
Non-solar heat flux	WRF	MITgcm Non-penetrative component of the air-sea heat flux computed from longwave radiation, sensible, and latent heat fluxes
Atmospheric surface pressure	WRF	MITgcm
Surface runoff	WRF	HD From the NOAH-MP land model
Subsurface runoff	WRF	HD From the NOAH-MP land model
Discharge at the river mouth	HD	MITgcm Remapped and spread over the MITgcm gridpoints

Table 2. List of the variables exchanged through the RegESM coupler between the different model components

This project has received funding from the European Union's Horizon 2020 research and innovation programme under grant agreement No. 101003598

The model domain covers the Med-CORDEX region (Fig. 1). The horizontal resolution is 12 km for the atmospheric component, 1/12° (~10 km) for the oceanic component, and 0.5° for the river routing model.

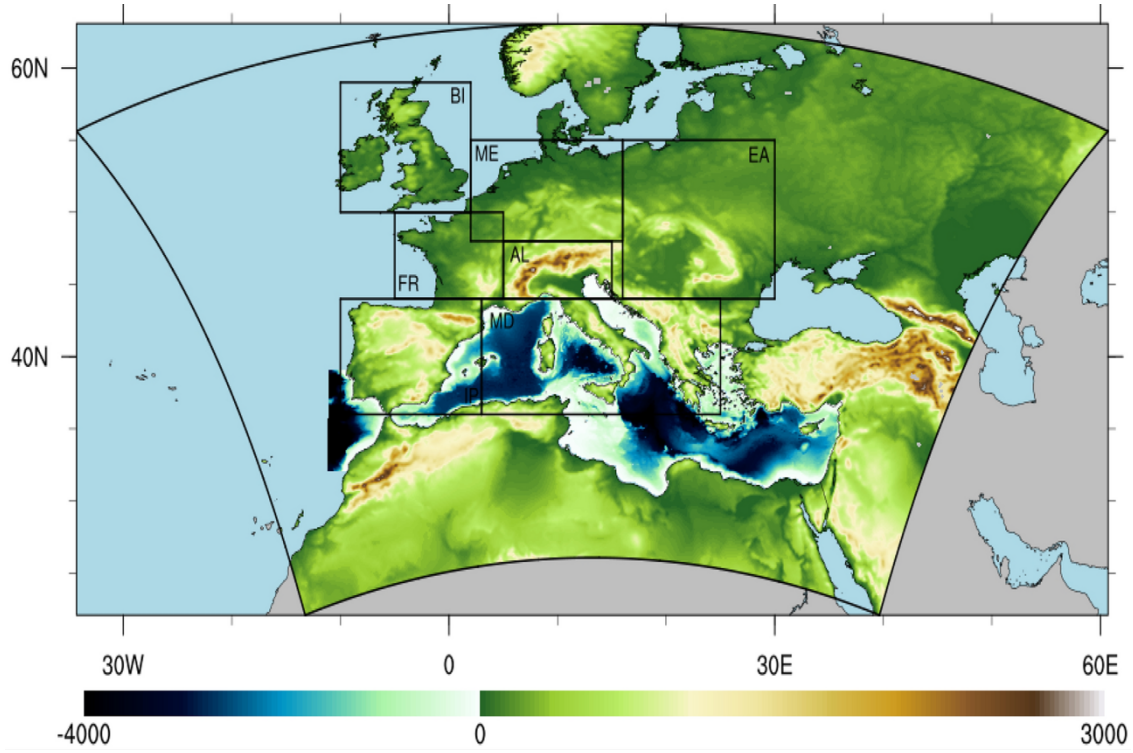

Figure 1. Domain used for the ENEA-REG simulations; the area defined by the black solid line represents the computational domain of the atmospheric model, with green shading highlighting the topography. The ocean domain is defined by the blue shading, used to represent bathymetry. Black boxes indicate seven regions, defined in the frame of the PRUDENCE project (Christensen and Christensen 2007), which are widely used for evaluation of climate models over Europe; they are: the Alps (AL), the British Isles (BI), Eastern Europe (EA), France (FR), the Iberian Peninsula (IP), the Mediterranean (MD), and Mid-Europe (ME).

In CoCliCo has been performed a hindcast simulation initialized and forced using ERA5 reanalysis (Hersbach et al., 2020) for the atmosphere and ORAS5 reanalysis (Zuo et al., 2019) for the ocean. Additionally, historical and three CMIP6 global scenario simulations (SSP1-2.6, SSP2-4.5, and SSP5-8.5; Eyring et al., 2016; O'Neill et al., 2016) are downscaled. The CMIP6 MPI-ESM1-2-HR (Gutjahr et al., 2019) serves as the driving global model, configured with a T127 atmospheric resolution (~0.93° or 103 km) and TP04 oceanic resolution (~0.4° or 44 km).

This project has received funding from the European Union's Horizon 2020 research and innovation programme under grant agreement No. 101003598

The MPI-ESM1-2-HR model was chosen due to its relatively high spatial resolution, well-balanced radiation budget, and explicitly tuned climate sensitivity of 3 K (Müller et al., 2018), making it suitable for prediction and impact studies. Present-climate experiments cover the period 1 August 1980–31 December 2014, while future simulations span 2015–2100.

Global ESMs often exhibit biases when compared to observations (Gleckler et al., 2008), and these biases can propagate into regional models, creating additional uncertainties in climate projections (Dosio, 2016). To mitigate this, bias correction techniques are commonly applied to global forcing data before dynamical downscaling. In this study, no bias correction is applied to the high-frequency (6-hourly) lateral boundary conditions of the MPI-ESM1-2-HR atmospheric component. However, monthly salinity, temperature, and elevation data used as open boundary conditions for the MITgcm ocean model are bias-corrected.

This differing treatment reflects the Mediterranean's thermohaline circulation, which is highly sensitive to variations in temperature and salinity from boundary conditions, particularly through the narrow Gibraltar Strait (Pinardi and Masetti, 2000). To avoid unrealistic Mediterranean circulation induced by biased CMIP6 forcing, the bias in ocean forcing data is corrected following the Med-CORDEX protocol (https://zenodo.org/record/8210985). This ensures that the simulated Mediterranean circulation is not degraded by spurious heat or salinity content. Post-simulation bias corrections of marine fields would not adequately recover such issues.

The oceanic bias correction follows Bruyère et al. (2014), which removes the mean bias of the driving model while preserving interannual variability and trends. Monthly data are decomposed into a mean seasonally varying climatological component and a perturbation term that includes high-frequency variability and climate-change trends. Similarly, ORAS5 reanalysis data are decomposed into a seasonally varying climatological mean and a perturbation term. Using this approach, present and future bias-corrected MPI-ESM1-2-HR boundary conditions are constructed by replacing the global model's climatological mean with that of the reanalysis.

2.2. Validation of ENEA REG Components

To evaluate the performance of the regional Earth System Model (ESM) in reproducing the mean annual cycle of surface air temperature, Figure 2 compares seasonal mean temperatures from the ENEA-REG hindcast and historical downscaling experiments to ERA5 reanalysis data using box plots. While ERA5, like other reanalysis products, is not fully observation-based, it is widely employed for validating climate models, particularly in downscaling experiments, as it enables assessment of the model's ability to replicate parent data (Mooney et al., 2013). In addition to the regional model simulations, we include the driving model (MPI-ESM1.2-HR) and the ensemble mean

This project has received funding from the European Union's Horizon 2020 research and innovation programme under grant agreement No. 101003598

of 25 CMIP6 ESMs in the analysis. Means, medians, and percentiles, computed for 1982–2014, are spatially aggregated across the sub-domains used in the PRUDENCE project (Christensen and Christensen, 2007).

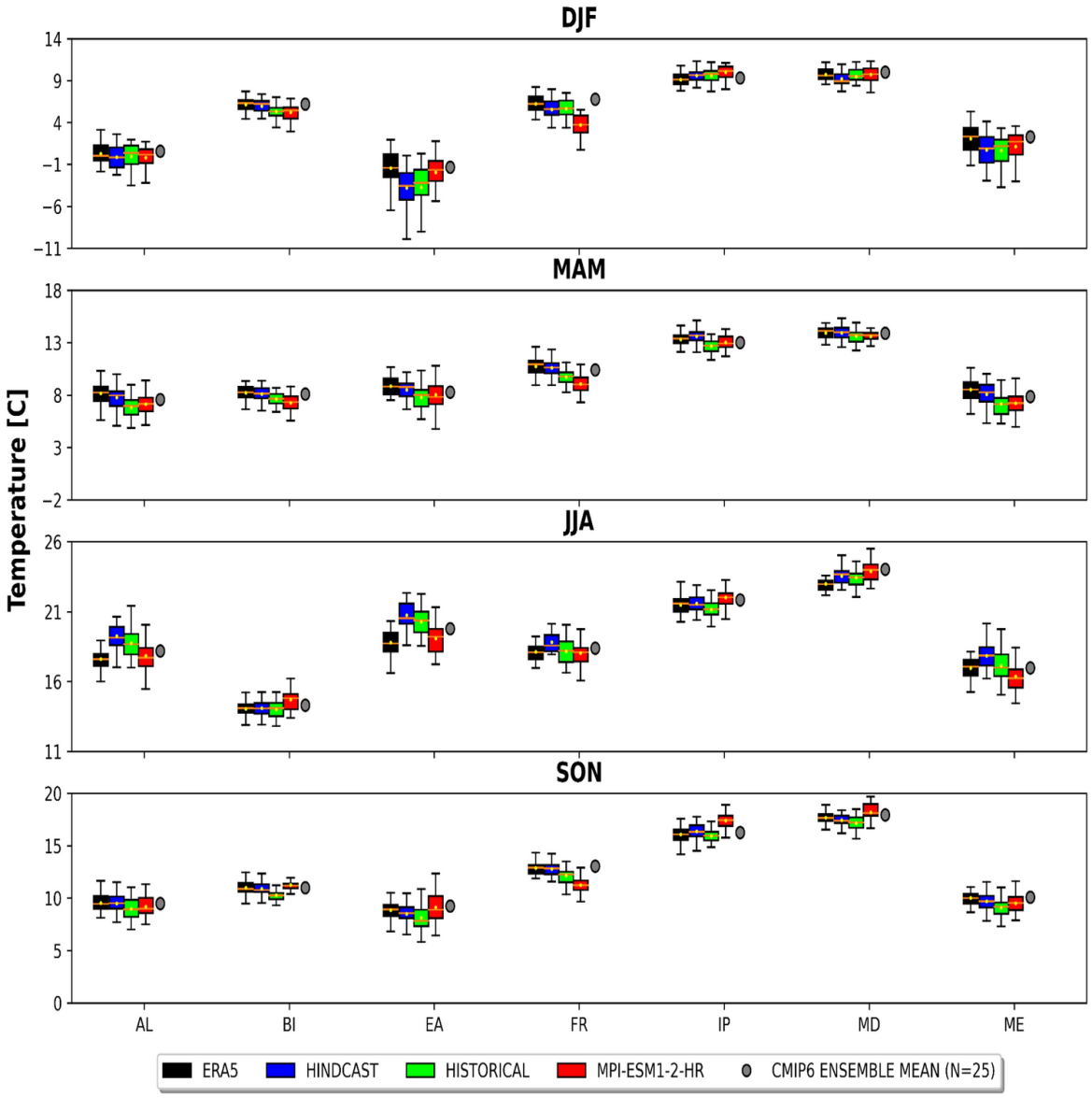

Figure 2. Mean seasonal (winter, spring, summer, and fall) near-surface air temperature spatially averaged over the PRUDENCE regions from: reference data (ERA5, black boxes), the ENEA-REG hindcast (blue boxes) and historical simulations (green boxes), the driving model of the historical experiment (i.e. MPI-ESM1-2-HR, red boxes) and the ensemble mean of 25 CMIP6 models (gray circle). The orange lines within the boxes represent the median of the temperature while the yellow circles are used to indicate the mean value. The seasonal averages are computed over the period 1982–2014

This project has received funding from the European Union's Horizon 2020 research and innovation programme under grant agreement No. 101003598

The results indicate that the downscaling experiments generally reproduce the seasonal temperature climatology well across PRUDENCE regions, despite notable biases in certain domains and seasons. For instance, the largest deviations from ERA5 occur during winter (DJF, December–January–February) in Eastern Europe (EA), where the model exhibits a cold bias of −2.3°C in both simulations. This bias, previously reported in other studies, is linked to deficiencies in simulating surface temperatures over snow-covered and wooded areas (e.g., Mooney et al., 2013; García-Díez et al., 2015; Katragkou et al., 2015). According to Varga and Breuer (2020), this bias stems primarily from an overestimation of snow depth caused by excessive snowfall and insufficient melting.

In summer (JJA, June–July–August), the downscaling experiments are systematically warmer than ERA5 in several sub-domains, with the most pronounced biases in the Alpine region (1.6°C in the hindcast and 1.1°C in the historical simulation) and Eastern Europe (1.9°C in the hindcast and 1.5°C in the historical). During spring (MAM, March–April–May), the hindcast exhibits minimal bias (maximum cold bias of −0.4°C in mid-Europe), whereas the historical simulation displays a cold bias exceeding −1°C in several sub-domains (e.g., Alps, Eastern Europe, France, and mid-Europe). Similarly, in fall (SON, September–October–November), the hindcast aligns closely with ERA5 (largest biases: −0.4°C in Eastern Europe and −0.3°C in mid-Europe), while the historical simulation exhibits a consistent cold bias across all sub-regions, with the largest discrepancy in mid-Europe (−1°C). This cold bias in the historical simulation appears to be inherited from the driving MPI ESM1.2 HR global model.

For CMIP6 models, it is well-documented that the multi-model ensemble mean often outperforms individual models in terms of bias reduction (e.g., Gleckler et al., 2008). Our findings confirm that the CMIP6 ensemble mean aligns more closely with ERA5 than the single MPI ESM1.2 HR model. Notably, in some regions (e.g., France, Iberian Peninsula, and the Mediterranean), the coarse MPI ESM1.2 HR exhibits significant biases relative to reference data, while its ENEA REG downscaling matches observations well. This underscores the advantage of regional downscaling over complex terrains like the Mediterranean basin.

The spatial variability of surface temperature simulated by ENEA REG was assessed using pattern correlations over PRUDENCE domains, with ERA5 as a reference (Fig. 3).

This project has received funding from the European Union's Horizon 2020 research and innovation programme under grant agreement No. 101003598

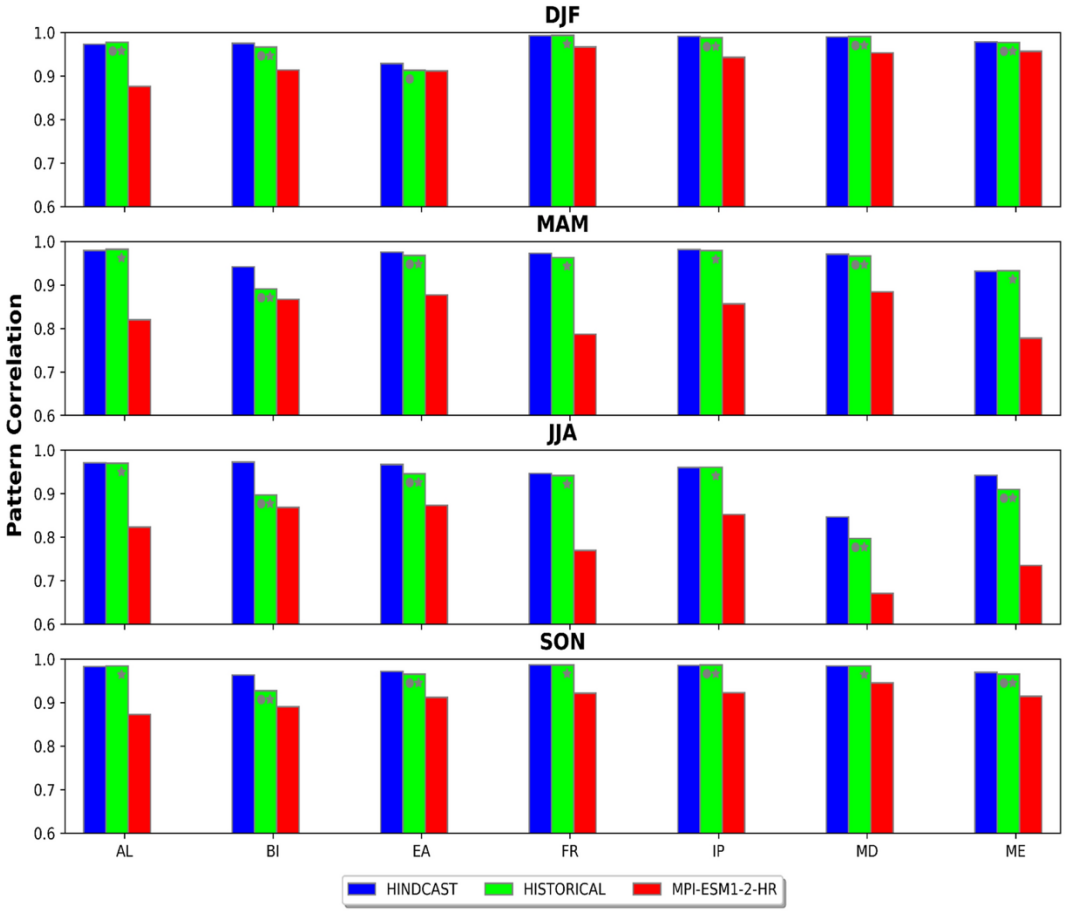

Figure 3. Centered pattern correlation between the surface air temperature from the reference data (i.e. ERA5) and the ENEA-REG hindcast (blue boxes) and historical simulations (green boxes); besides, we also show the pattern correlation for MPI-ESM1-2-HR (red boxes) which has been used to drive the historical experiment. The seasonal patterns are computed for the reference period 1982–2014 over the PRUDENCE sub-regions (Christensen and Christensen 2007). In this analysis the two WRF experiments, and the global MPI-ESM1-2-HR model have been regridded to the ERA5 grid. 1% level significance of pattern correlation difference between the historical and the hindcast simulation (gray circles) and between the historical and the global model simulation (gray stars) has been assessed by bootstrap procedure with 1000 repetitions

We also evaluated the significance of pattern correlation differences between the historical and hindcast simulations (gray circles in Fig. 3) and between the historical simulation and its driving model (gray stars in Fig. 3) using a Monte Carlo bootstrap procedure (Wilks, 2011). Results show that ENEA REG historical and hindcast simulations align well with ERA5 for all domains, while MPI ESM1 2 HR pattern correlations are significantly lower, except in EA during DJF. Furthermore, no significant differences were observed in spatial patterns between the hindcast and historical simulations, whereas the historical simulation significantly outperforms its

This project has received funding from the European Union's Horizon 2020 research and innovation programme under grant agreement No. 101003598

global forcing. These results highlight the importance of local features and resolution over the type of forcing used for downscaling. The improved performance of ENEA - REG compared to its driving ESM is attributed to the finer spatial grid, which resolves heterogeneous surface features such as land cover, complex topography, and land-sea contrasts.

Inter-annual variability was analyzed using the Model Variability Index (MVI; Gleckler et al., 2008), which compares standard deviation differences between the model and reference data. A threshold value of 0.5 was suggested by Scherrer (2011) to indicate good variability representation. Seasonal MVIs for surface temperature (Fig. 4) show that the hindcast accurately reproduces observational variability across all seasons, whereas the historical simulation tends to inherit variability from the global forcing, especially in seasons dominated by synoptic boundary conditions. Improvements in MVI are evident over the Mediterranean region, particularly in summer (JJA), when local circulations and small-scale processes are better resolved. In the Balkan region during winter (DJF) and Northern Africa during summer (JJA), the historical simulation amplifies variability compared to ERA5, suggesting misrepresentation of local processes in the regional model. The discrepancy in the Balkan region during DJF may be linked to the interplay between the persistent Eastern European cold bias and frequent North-Eastern outbreaks of cold air, which enhance temperature variability (Varga and Breuer, 2020).

This project has received funding from the European Union's Horizon 2020 research and innovation programme under grant agreement No. 101003598

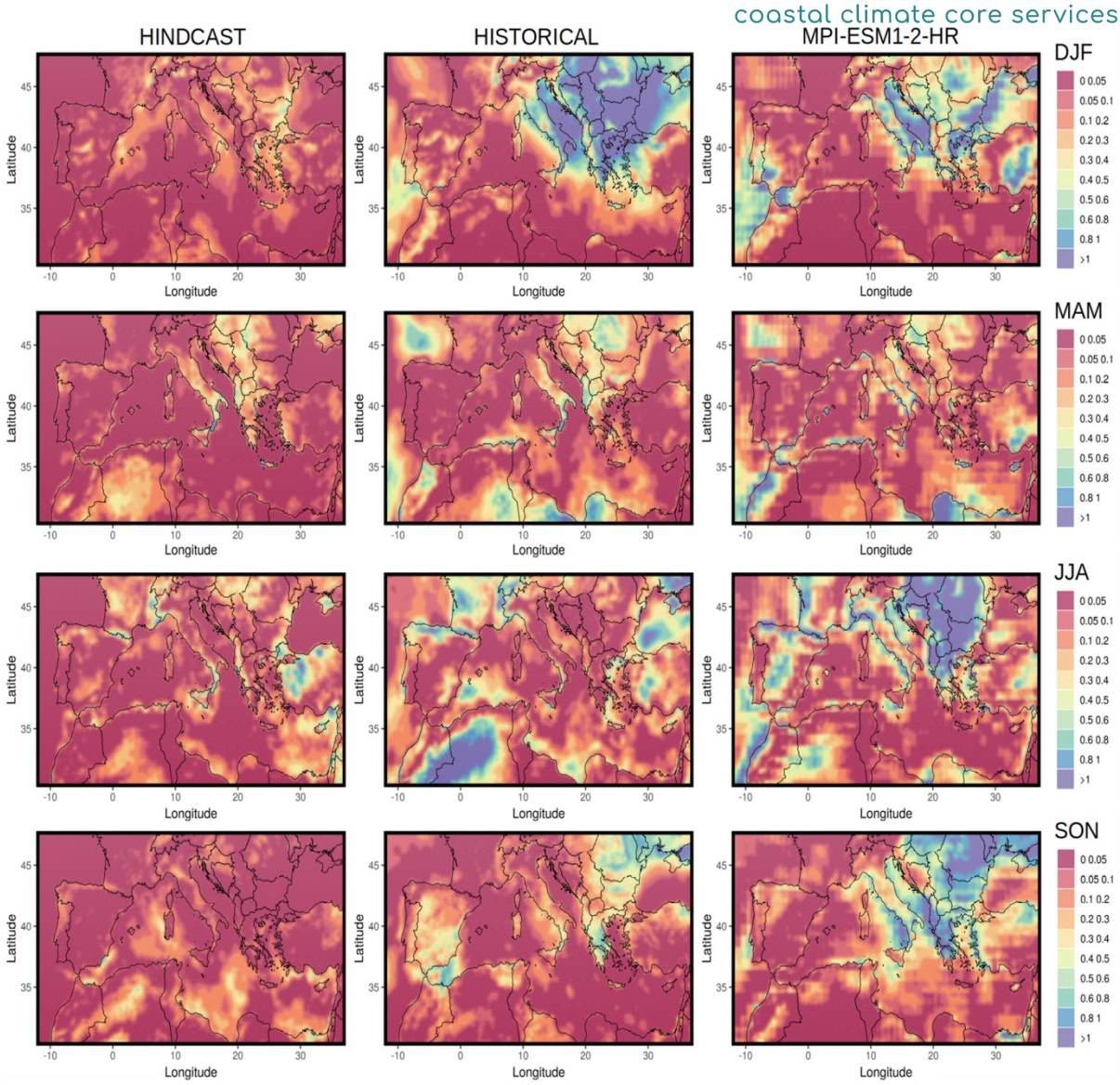

Figure 4. Model Variability Index (MVI) of near-surface air temperature for the ENEA_REG hindcast simulation (left column), the ENEA-REG historical simulation (central column) and the MPI-ESM1-2-HR simulation (right column). Boreal winter DJF (first row), spring MAM (second row), summer JJA (third row), autumn SON (fourth row)

Figure 5 compares seasonal precipitation from ENEA REG downscaling experiments with ERA5 data. The hindcast agrees well with ERA5 in winter, showing the largest dry bias (−0.2 mm/day) in the Alpine and Mediterranean regions. Conversely, the historical run is wetter than ERA5, with biases of 1.5 mm/day in the Alps, 1.3 mm/day in France, and 1.1 mm/day in the Iberian Peninsula. During MAM, the hindcast is consistently drier than ERA5, with the largest bias (−0.54 mm/day) in the Alps, while

This project has received funding from the European Union's Horizon 2020 research and innovation programme under grant agreement No. 101003598

the historical simulation is wetter, particularly in France (0.76 mm/day) and the Alps (0.6 mm/day). In summer, both simulations are drier than ERA5, with the largest biases in the Alps (hindcast: −1.2 mm/day; historical: −0.75 mm/day). During SON, the two simulations align closely with ERA5, with minor biases (e.g., −0.58 mm/day in the Alps for the hindcast).

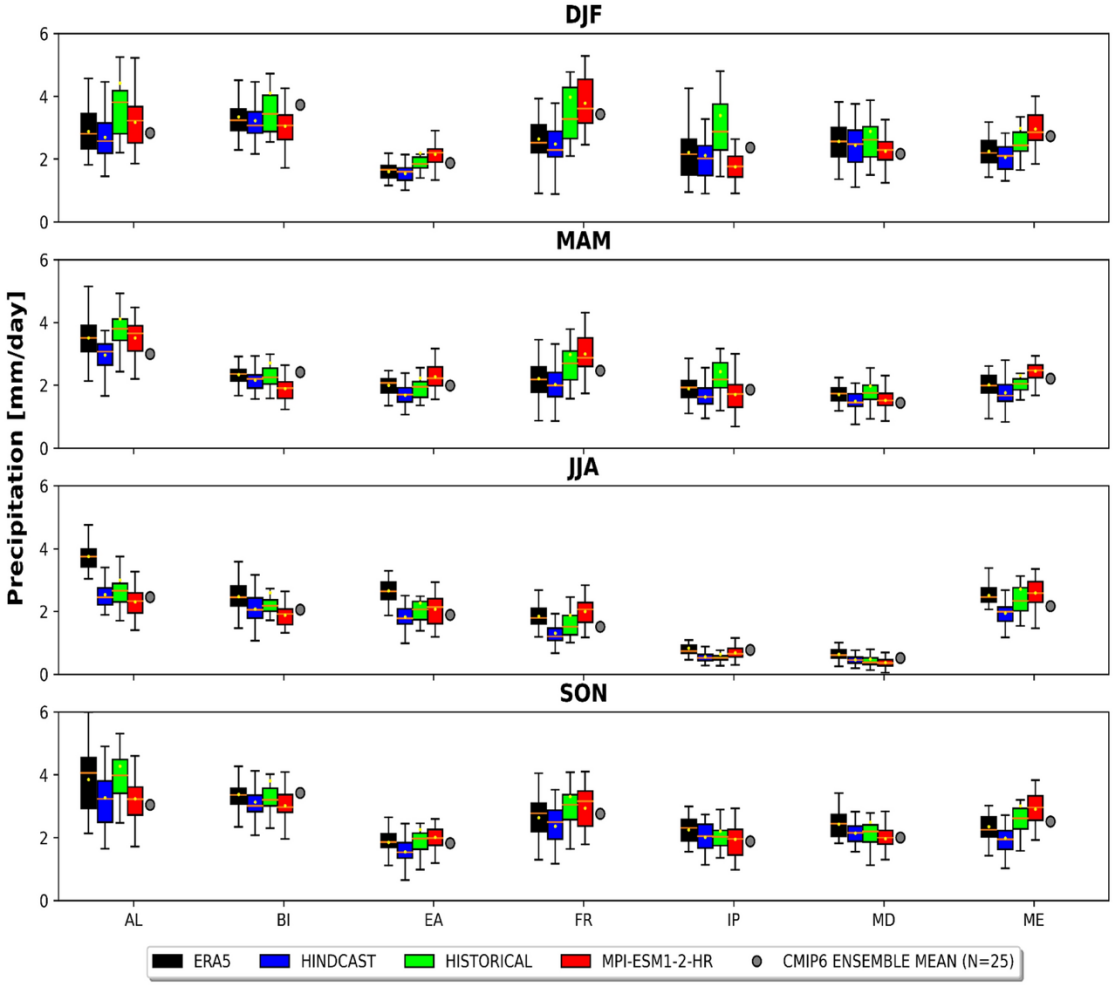

Figure 5. As Fig. 2, but for precipitation

Pattern correlations for precipitation (Fig. 6) are consistent with those for surface temperature but generally lower, particularly in the Alpine region during SON, where the historical simulation achieves a correlation of 0.5. The historical run significantly outperforms MPI ESM1 2 HR in all regions and seasons, reflecting the benefits of high-resolution downscaling, especially in complex terrain. The high-resolution ocean coupling in ENEA REG likely contributes to improved precipitation patterns over the Mediterranean domain, as discussed in Sect. 3.2.

This project has received funding from the European Union's Horizon 2020 research and innovation programme under grant agreement No. 101003598

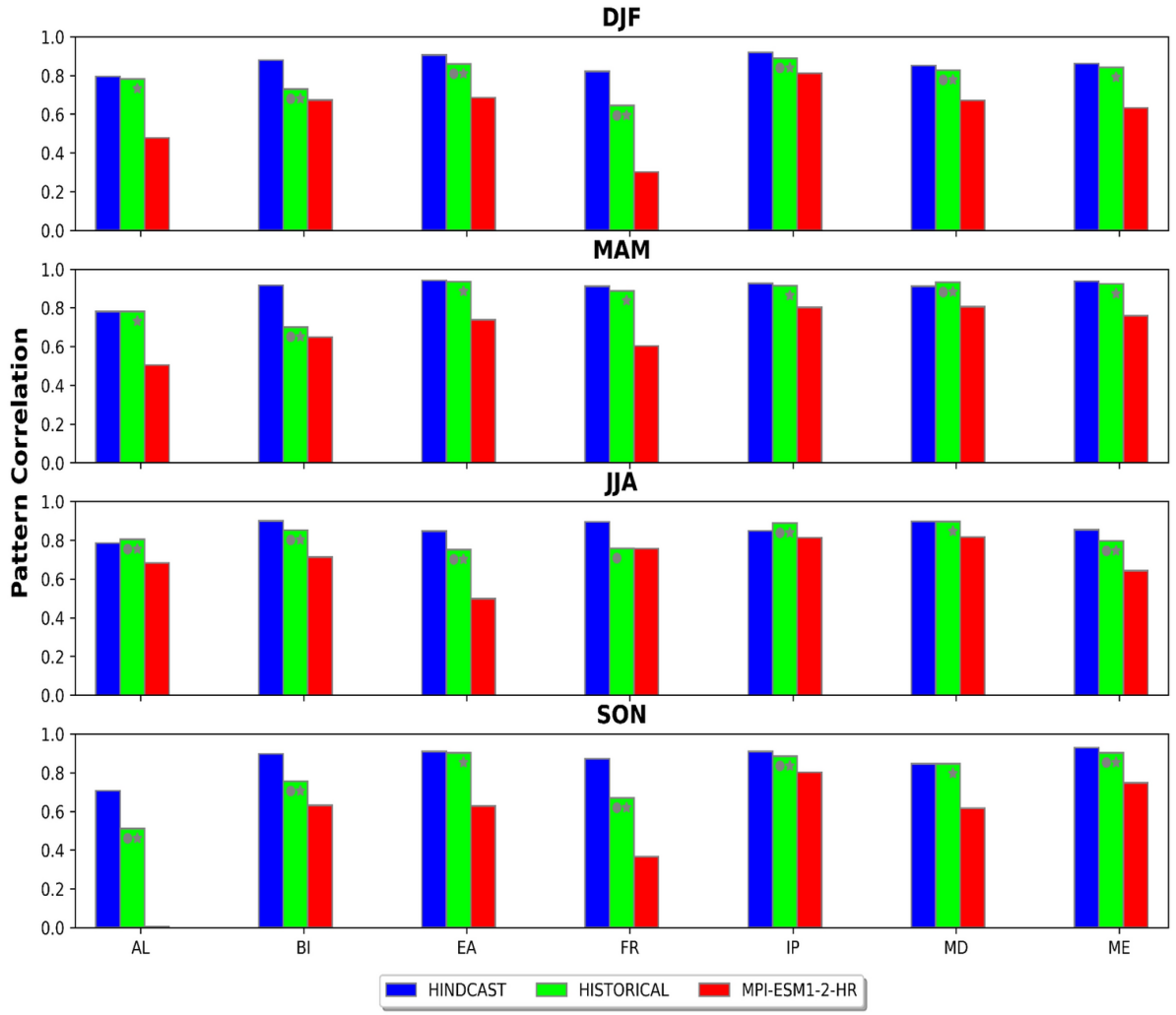

Figure 6. As Fig. 3, but for precipitation

The precipitation MVI (Fig. 7) reveals fair agreement between downscaling experiments and ERA5, excluding summer, where near-zero precipitation around the Mediterranean leads to MVI values exceeding 1. Unlike surface temperature, precipitation variability in ENEA REG closely follows its forcing, highlighting limitations of the regional model's 12-km resolution in resolving convective structures. Transitioning to convection-permitting resolutions is expected to enhance precipitation variability representation, particularly in summer.

This project has received funding from the European Union's Horizon 2020 research and innovation programme under grant agreement No. 101003598

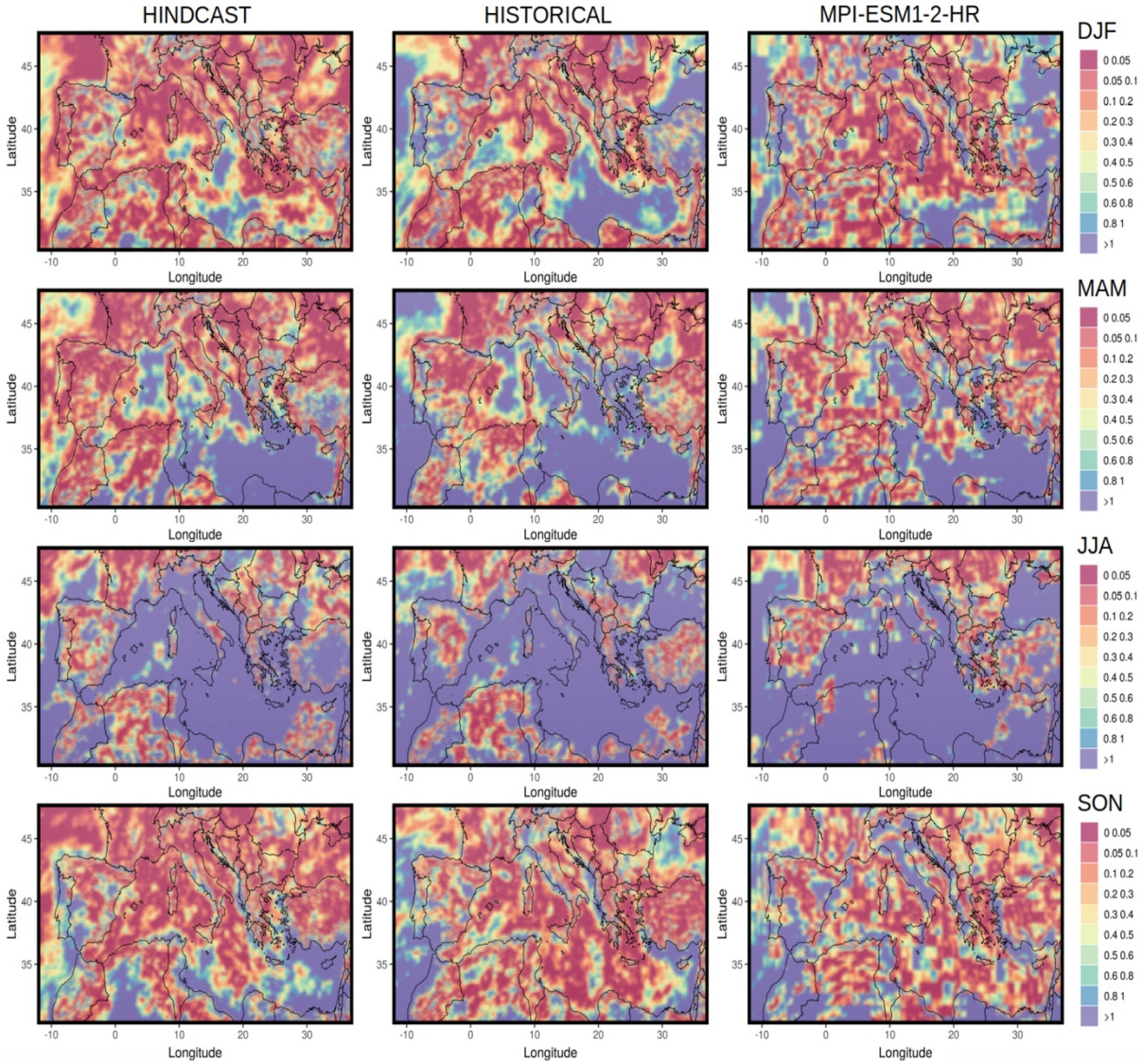

Figure 7. Model Variability Index (MVI) of Precipitation for the ENEA-REG hindcast simulation (left column), the ENEA-REG historical simulation (central column) and the MPI-ESM1-2-HR simulation (right column). Boreal winter DJF (first row), spring MAM (second row), summer JJA (third row), autumn SON (fourth row)

SST climatologies from the ENEA-REG hindcast and historical experiments are compared to satellite-based observations (SST_MED_SST_L4_REP_OBSERVATIONS_010_021) obtained from the Copernicus Marine Service (CMEMS). Figure 8 shows similar SST bias patterns between the hindcast and historical runs, though the historical simulation is systematically colder. Both simulations exhibit positive biases in winter and negative biases in summer, reflecting a reduced amplitude of the seasonal cycle. In contrast,

This project has received funding from the European Union's Horizon 2020 research and innovation programme under grant agreement No. 101003598

the driving global ESM shows a less consistent bias pattern, likely due to its coarse resolution and inability to capture small-scale features.

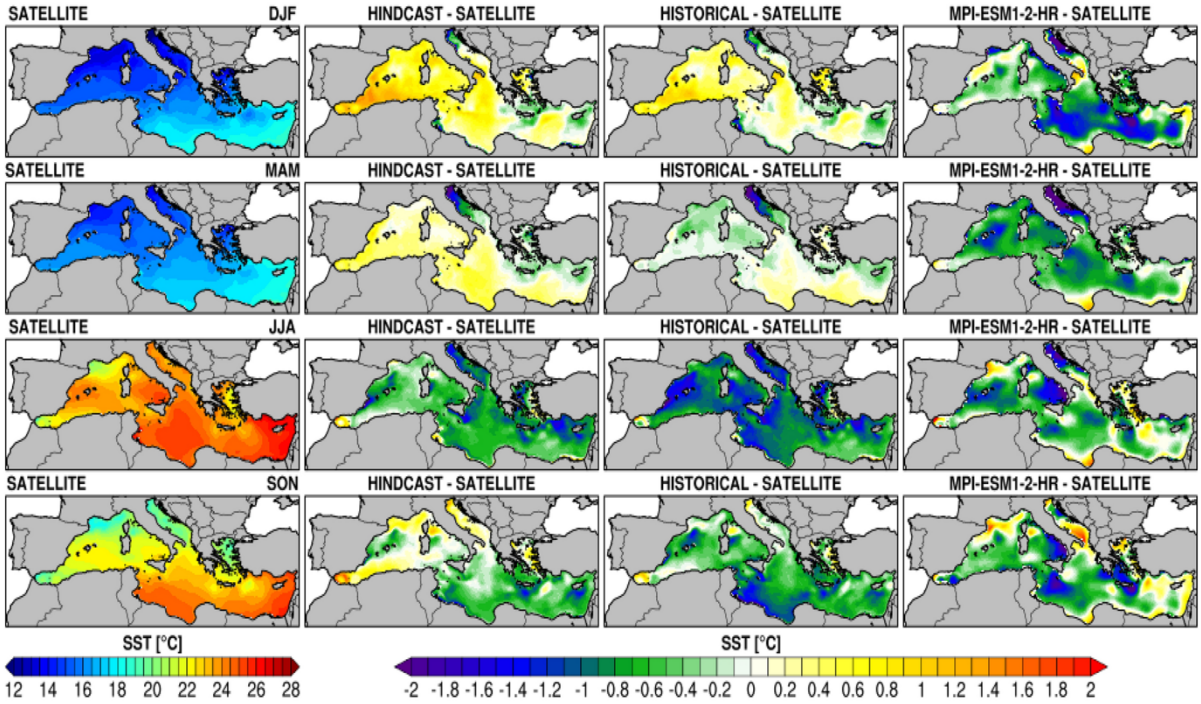

Figure 8. Comparison of seasonal sea surface temperature from satellite data, the ENEA-REG hindcast and historical experiments and the MPI-ESM1-2-HR model. Seasonal averages are computed for the period 1982–2014

The vertical structure of temperature and salinity, averaged over the Mediterranean basin and its sub-basins (WMED and EMED), is presented in Table 3. Results indicate good agreement with reanalysis data for both simulations, with the hindcast slightly warmer and saltier than the reference, particularly in the EMED. The historical run shows a reduced bias in the western basin's upper layer compared to the hindcast.

Depth (m)	Parameter	MED	WMED	EMED
0–150	Temperature	16.65	15.41	17.33
		0.09	0.43	-0.08

This project has received funding from the European Union's Horizon 2020 research and innovation programme under grant agreement No. 101003598

		-0.04	0.15	-0.12
150–600	Temperature	14.05	13.46	14.41
		0.25	0.30	0.21
		0.33	0.25	0.38
600–3500	Temperature	13.35	12.96	13.57
		0.27	0.15	0.36
		0.25	0.13	0.34
0–150	Salinity	38.41	37.85	38.73
		0.18	0.04	0.22
		0.15	-0.01	0.22
150–600	Salinity	38.82	38.50	38.85
		0.02	0.04	0.17
		0.04	0.02	0.21
600–3500	Salinity	38.66	38.48	38.81
		0.12	0.03	0.12
		0.11	0.02	0.12

Table 3. Average Temperature (°C) and Salinity (psu) at various depths for the whole Mediterranean (MED), the Western (WMED) and the Eastern (EMED) sub-basins

Sea surface elevation and circulation, compared to satellite-derived Mean Dynamic Topography (MDT), exhibit good spatial agreement, with large-scale features well represented in both simulations (Fig. 9). The Atlantic water stream and associated currents, cyclonic circulations in the WMED, and gyres in the Adriatic Sea are accurately resolved. However, weaker anticyclonic anomalies in the Alborán and Levantine Seas and discrepancies in the northern Aegean require further investigation.

This project has received funding from the European Union's Horizon 2020 research and innovation programme under grant agreement No. 101003598

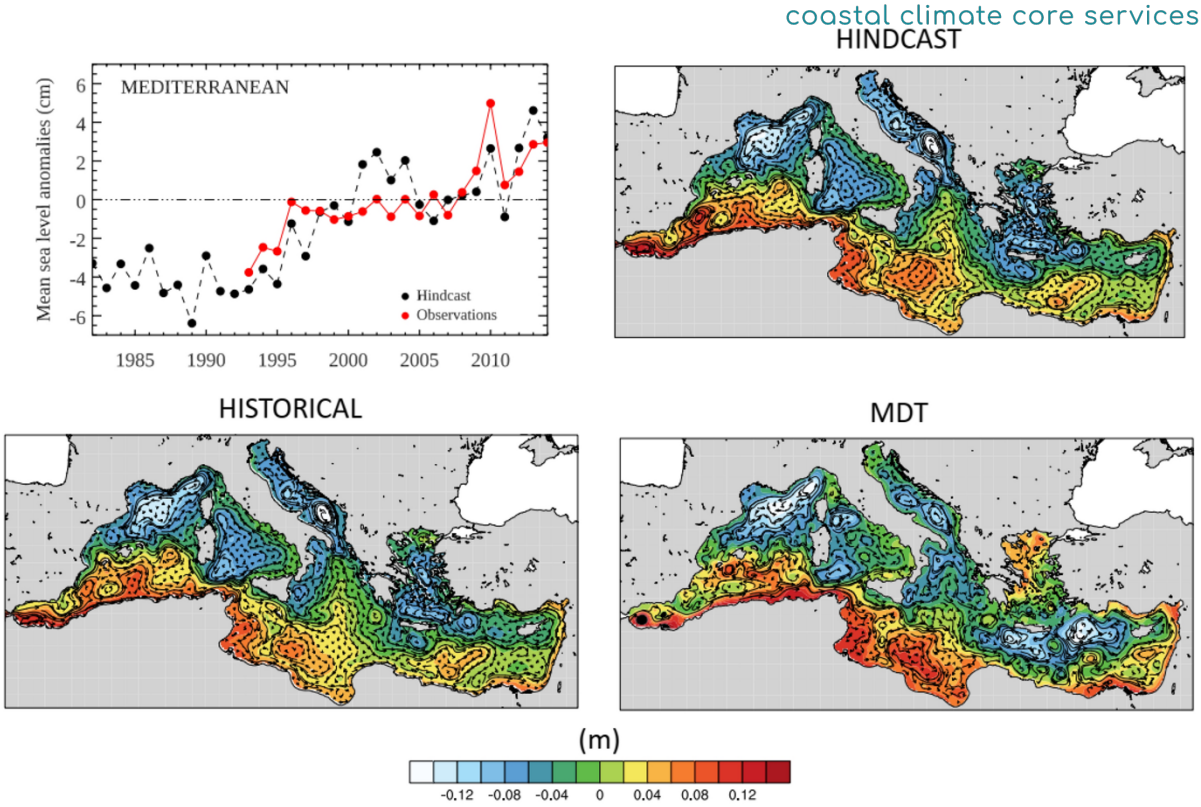

Figure 9. The maps show the average sea level as simulated by the hindcast and historical experiments (1982–2014 average) and the satellite observations (1993–2014 average). The average circulation at 30 m of depth has been superimposed on the elevation in the two ENEA-REG simulations, while a geostrophic reconstruction of the circulation has been used in the case of the MDT (also provided by CMEMS). In the top left panel, the annual time series of the average basin elevation from the hindcast (black dots) is compared with that resulting from the observations (red dots).

The hindcast captures inter-annual variability in basin elevation well, including observed trends and variability from 1993–2014, although discrepancies occur in the early 2000s, likely due to strong atmospheric anomalies during this period (e.g., the 2003 heatwave). Overall, ENEA REG reproduces large-scale oceanic processes effectively, with regional refinements improving upon its global forcing model.

2.3. 21st-Century Projections

This section presents key findings from simulations conducted with ENEA-REG, focusing on projected changes in Essential Climate Variables (ECVs) and Essential Ocean Variables (EOVs). Figure 10 illustrates the temporal evolution of annual near-surface air temperature and sea surface temperature (SST) averaged over the

This project has received funding from the European Union's Horizon 2020 research and innovation programme under grant agreement No. 101003598

Mediterranean basin (sea only) as simulated by ENEA-REG. These results are compared with global driver simulations and observational datasets for reference. During the historical period, the ENEA-REG hindcast simulation slightly amplifies the 2004–2005 SST minimum (García-Monteiro et al., 2022) following the 2003 heatwave. Subsequently, the oceanic component of the model exhibits a cold bias (Fig. 10b), also visible but weaker in the 2 m air temperature (Fig. 10a). This feature, noted in early Med-CORDEX coupled simulations by Ruti et al. (2016) and more recently by Storto et al. (2023), persists here. Future projections indicate that while the three scenarios remain similar in the early 21st century, divergence occurs after 2050, with a temperature difference of approximately 2 °C by the century's end between SSP2-4.5 and SSP5-8.5. The regional simulations align with their global counterparts but show weaker trends in SSP2-4.5 and SSP5-8.5 for air surface temperature and SST. Consistent with global forcing, no significant warming is observed in SSP1-2.6.

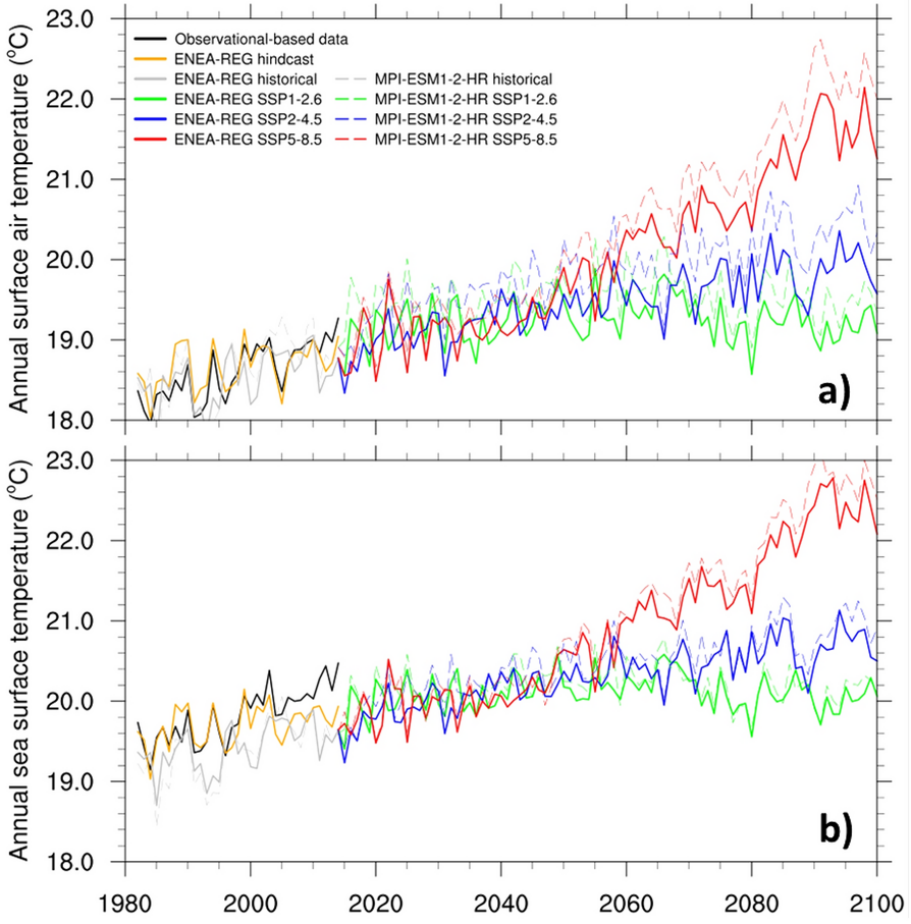

Figure 10. Annual time series of near-surface air temperature (a) and Sea Surface temperature (b) (°C) from the ENEA-REG scenario simulations averaged over the entire Mediterranean basin

This project has received funding from the European Union's Horizon 2020 research and innovation programme under grant agreement No. 101003598

Figure 11 displays spatial patterns of air surface temperature changes for the three scenarios, comparing the late 21st century to the historical period. Consistent with global trends (Tebaldi et al., 2020), warming over the Mediterranean is more pronounced over land than sea. Summer sees the greatest changes under SSP5-8.5, with temperature increases reaching 5 °C in the Iberian Peninsula and North Africa. In contrast, the Tyrrhenian Sea and the eastern Mediterranean basin show increases up to 2.5 °C, while the Adriatic experiences rises of up to 4 °C during SON. Winter warming predominantly affects Eastern Europe. The SSP2-4.5 scenario exhibits similar spatial patterns but with weaker warming, averaging around 1.5 °C. In SSP1-2.6, only limited areas, such as Eastern Europe in winter and northern Africa in summer, show warming of up to 2 °C.

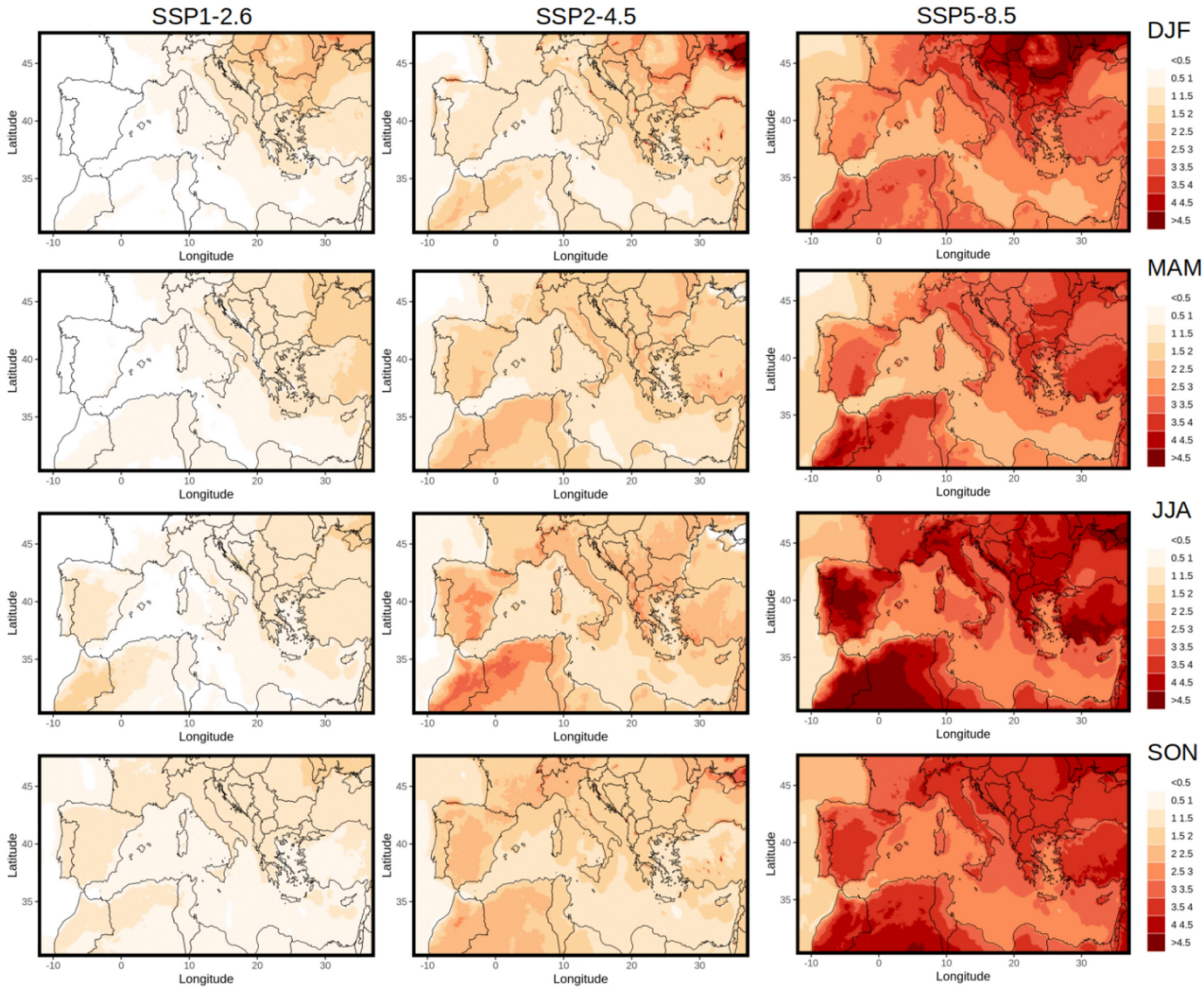

Figure 11. Near-surface air temperature (K) projected climate change (2071–2100 minus 1985–2014) from the ENEA-REG scenario simulations: SSP1-2.6 (left column), SSP2-4.5 (central column) and SSP5-8.5 (right column). Boreal winter DJF (first row), spring MAM (second row), summer JJA (third row), autumn SON (fourth row). Values at all grid points are significant at 10% level. Significance assessed by bootstrap procedure with 1000 repetitions

This project has received funding from the European Union's Horizon 2020 research and innovation programme under grant agreement No. 101003598

Regarding mean precipitation (Fig. 12), ENEA-REG simulates significant reductions over the Mediterranean in SSP5-8.5 and SSP2-4.5 during all seasons, with the largest decreases in SON for SSP1-2.6. A consistent pattern emerges across scenarios: summer precipitation decreases, especially in the western domain and over the Balkan Peninsula, while winter and spring see increases in central and western Europe. These trends align with the latest IPCC report (IPCC, 2022) and annual mean trends reported by Zittis et al. (2019).

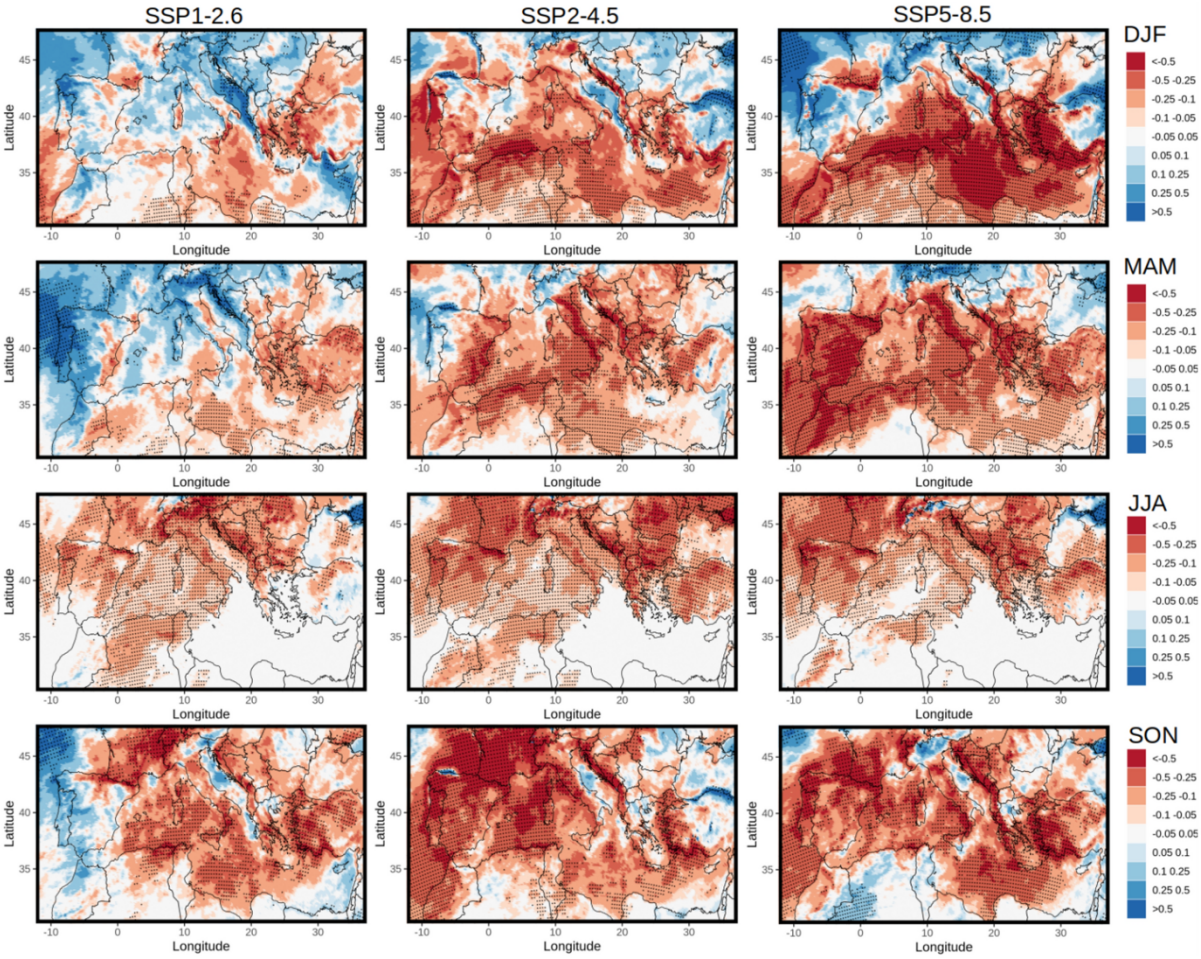

Figure 12. Precipitation (mm d–1) projected climate change (2071–2100 minus 1985–2014) from the ENEA-REG scenario simulations: SSP1-2.6 (left column), SSP2-4.5 (central column) and SSP5-8.5 (right column). Boreal winter DJF (first row), spring MAM (second row), summer JJA (third row), autumn SON (fourth row). Black dots indicate 10% level significance, assessed by bootstrap procedure with 1000 repetitions

This project has received funding from the European Union's Horizon 2020 research and innovation programme under grant agreement No. 101003598

The oceanic component of ENEA-REG reveals changes in temperature and salinity profiles for the three scenarios (Tables 4 and 5). Two 20-year periods (2046–2065 and 2081–2100) are analyzed to capture mid- and long-term changes relative to the historical simulation. By mid-century, surface and intermediate layers show temperature anomalies increasing with scenario severity, reaching 1 °C. Anomalies in deeper layers are smaller and scenario-independent. Regional differences are evident, with higher surface anomalies in the eastern basin and elevated intermediate anomalies in the west, possibly linked to surface heat surplus propagation or inflow of warmer Levantine Intermediate Water (LIW). Salinity anomalies indicate stronger stratification, with negative values in the upper layer and positive values below. By century's end, temperature anomalies increase across all layers and scenarios, except for a slight decrease in SSP1-2.6's upper layer. Under SSP5-8.5, surface and intermediate anomalies more than double compared to mid-century, with eastern upper-layer anomalies reaching 2.6 °C. Figure 10 corroborates this trend, showing accelerated SST increases after 2060.

		Depth (m)		
		0–150	150–600	600–3500
BASIN	**SCENARIO**	**TEMPERATURE**		
MED	SSP126	0.73	0.88	0.47
	SSP245	0.85	0.97	0.45
	SSP585	1.07	1.00	0.46
WMED	SSP126	0.59	1.05	0.58
	SSP245	0.66	1.17	0.57
	SSP585	0.75	1.18	0.57
EMED	SSP126	0.81	0.79	0.40
	SSP245	0.95	0.85	0.37
	SSP585	1.25	0.89	0.39
BASIN	**SCENARIO**	**SALINITY**		

This project has received funding from the European Union's Horizon 2020 research and innovation programme under grant agreement No. 101003598

MED	SSP126	- 0.11	0.19	0.17
	SSP245	- 0.10	0.18	0.13
	SSP585	- 0.14	0.14	0.13
WMED	SSP126	- 0.22	0.23	0.16
	SSP245	- 0.24	0.23	0.14
	SSP585	- 0.28	0.20	0.14
EMED	SSP126	- 0.05	0.16	0.17
	SSP245	- 0.02	0.14	0.12
	SSP585	- 0.06	0.10	0.13

Table 4. Differences between values averaged over the period 2046–2065 of the three scenarios and the whole period (1985–2014) of the historical simulation. Averages are computed over the whole Mediterranean Sea (MED), and over the western and eastern sub-basins (WMED and EMED)

		Depth (m)		
		0–150	150–600	600–3500
BASIN	**SCENARIO**	**TEMPERATURE**		
MED	SSP126	0.61	0.91	0.66
	SSP245	1.05	1.11	0.61
	SSP585	2.45	2.08	0.68
WMED	SSP126	0.46	1.12	0.84
	SSP245	0.92	1.47	0.84
	SSP585	2.16	2.40	0.88
EMED	SSP126	0.70	0.78	0.55
	SSP245	1.12	0.89	0.46
	SSP585	2.62	1.89	0.56

This project has received funding from the European Union's Horizon 2020 research and innovation programme under grant agreement No. 101003598

BASIN	SCENARIO	SALINITY		
MED	SSP126	−0.15	0.08	0.18
	SSP245	−0.27	0.06	0.15
	SSP585	−0.06	0.22	0.16
WMED	SSP126	−0.21	0.16	0.19
	SSP245	−0.38	0.19	0.18
	SSP585	−0.27	0.33	0.18
EMED	SSP126	−0.12	0.03	0.17
	SSP245	−0.21	−0.01	0.13
	SSP585	0.06	0.16	0.15

Table 5. Differences between values averaged over period 2081–2100 of the three scenarios and the whole period (1981–2014) of the historical simulation. Averages are computed over the whole Mediterranean Sea (MED), and over the western and eastern sub-basins (WMED and EMED)

Projected sea level changes, primarily driven by thermal expansion, are depicted in Fig. 13. Results from MPI-ESM1-2-HR and ENEA-REG align with AR6 ensemble medians but diverge significantly in SSP5-8.5, where the regional and global means are approximately 10 cm lower than the AR6 median by 2100. Contributions to sea level rise include thermal expansion, melting of sea ice, glacier mass loss, land water storage changes, and vertical land motion, as detailed in IPCC AR6 (Fox-Kemper et al., 2021).

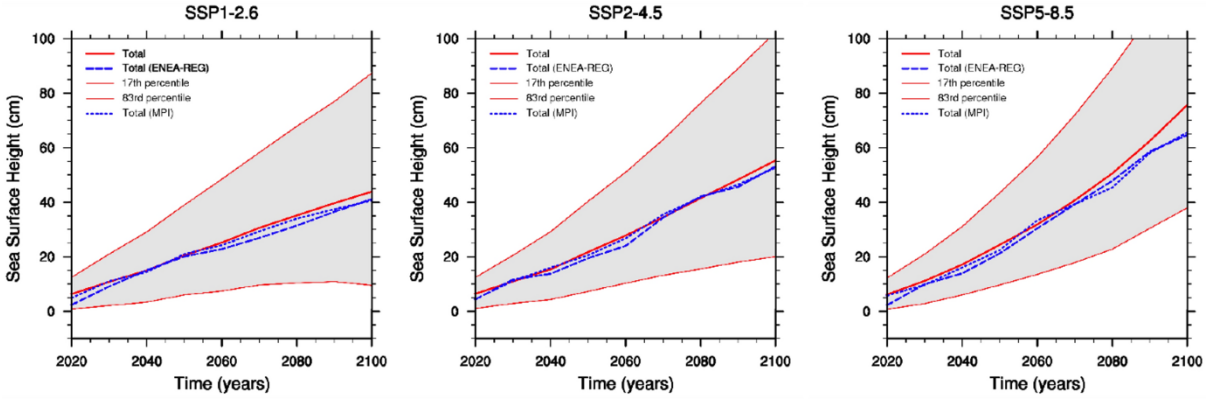

This project has received funding from the European Union's Horizon 2020 research and innovation programme under grant agreement No. 101003598

Figure 13. Change of the average total sea level over the Mediterranean basin for the three SSP scenarios (blue curves; dotted = MPI-ESM1-2-HR; dashed = ENEA-REG). The projections are relative to a 1995–2014 baseline. The thick red line is the median over the AR6 models and the shaded area corresponds to the 17th–83rd percentile range

Figure 14 highlights circulation-induced sea level patterns for the period 2096–2100 compared to 1995–2014. The regional model exhibits intensified east-west differences, with higher resolution capturing localized variations. For instance, in SSP5-8.5, the Balearic Islands display regional increases up to 30 cm, contrasting the global model's 10 cm. Negative anomalies in the Adriatic Sea from the global model correspond to higher positive anomalies in ENEA-REG, reflecting enhanced representation of circulation dynamics.

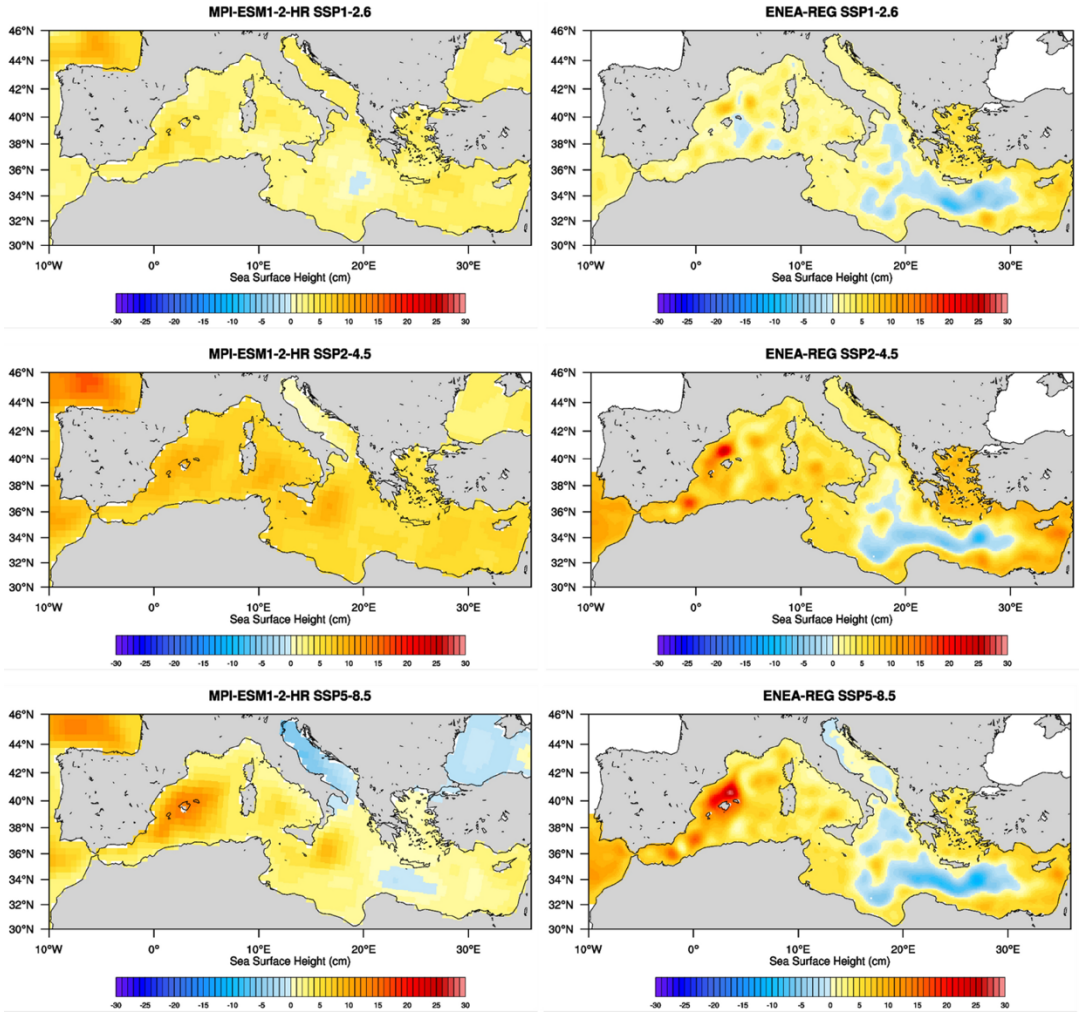

Figure 14. Sea surface height computed averaging the last five years of the simulations respect to the average over the historical period 1995–2014. Left panels for the MPI-ESM1-2-HR model, right panels ENEA-REG simulations. Only the circulation component is considered

This project has received funding from the European Union's Horizon 2020 research and innovation programme under grant agreement No. 101003598

Figure 15 presents monthly mean sea levels near key Italian ports (Genoa, Naples, and Venice), comparing global and regional simulations. In general, the regional model predicts slightly lower mean values but increased variability. For example, while Venice shows modest sea level changes under SSP1-2.6, more severe scenarios indicate rising extremes and higher risks of flooding. The greater variability in ENEA-REG suggests localized effects, such as storm surges and coastal inundations, could become more frequent, emphasizing the importance of high-resolution modeling for coastal impact assessments.

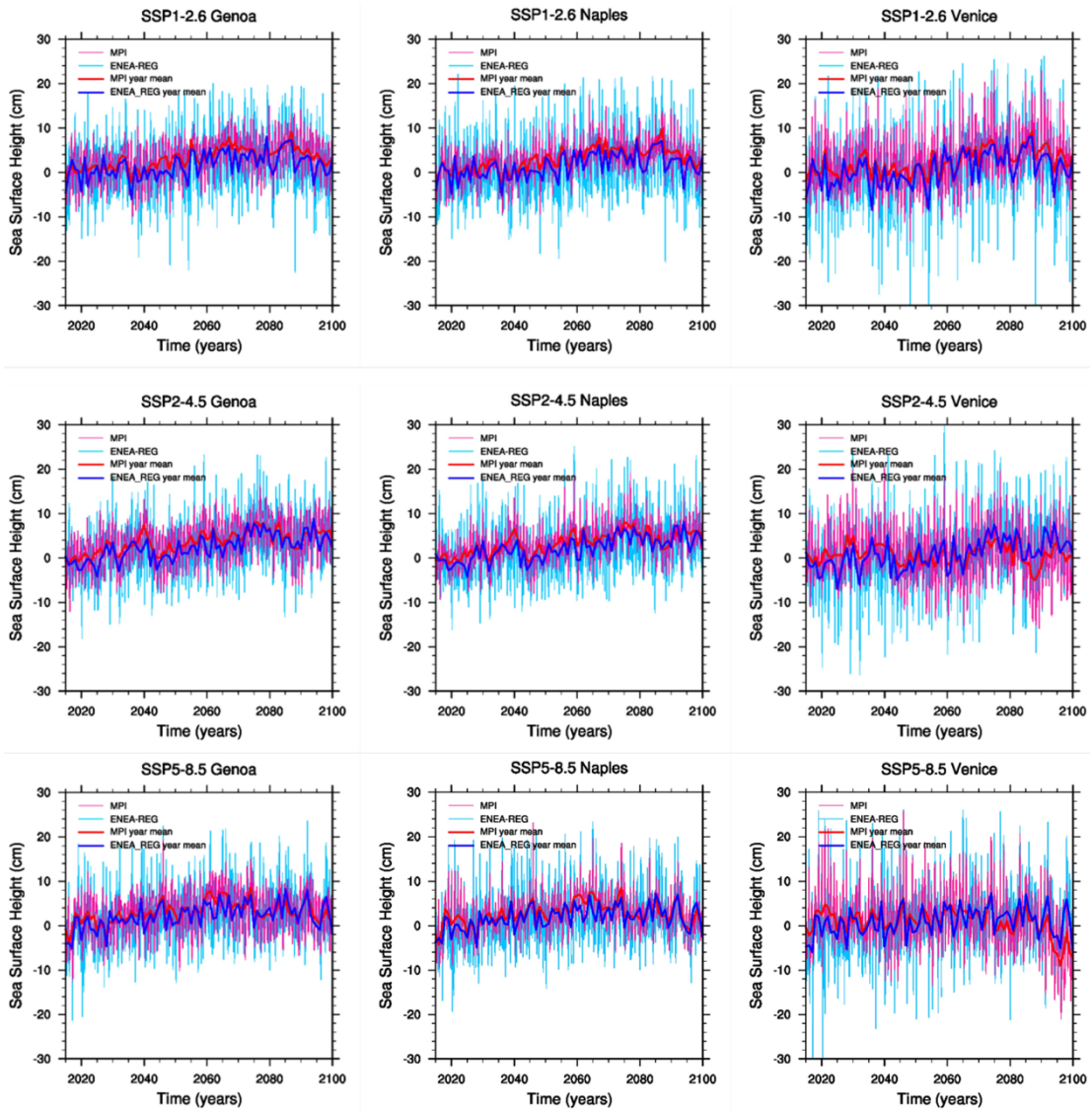

Figure 15. Comparison of the MPI-ESM1-2-HR (MPI) and ENEA-REG sea surface height for model points near to Genoa, Naples and Venice. From the left to the right column, scenario SSP1-2.6, SSP2-4.5 and SSP5-8.5. Monthly values and yearly means are shown. Values are computed with respect to the average over the 1995–2014 historical period

This project has received funding from the European Union's Horizon 2020 research and innovation programme under grant agreement No. 101003598

3. High resolution mean sea-level change hindcasts and projections on the European Continental Shelf

The Iberian–Biscay–Ireland (IBI) region, encompassing the northeastern Atlantic Ocean, the North Sea, and the western Mediterranean, represents a particularly challenging area for sea level projection due to its diverse bathymetry and dynamic oceanographic features. This region includes wide continental shelves in the North Sea and the English Channel, narrow shelves along the Iberian Peninsula, and complex interactions in the Strait of Gibraltar (Sotillo et al., 2015; Maraldi et al., 2013). Furthermore, it is subject to a variety of physical processes, including upwelling, slope currents, and mesoscale eddies. Existing GCM-based SL projections for the IBI region often exhibit significant biases, particularly in the Mediterranean Sea, where discrepancies in ocean salinity and temperature contribute to unrealistic SL trends (Levier et al., 2020).

3.1. The IBI-CCSv2 regional ocean model and methodology

To address these challenges, a specific ocean model called IBI-CCS (Iberian–Biscay–Ireland Climate Change Scenarios) model has been implemented. The IBI-CCS model is built on version 3.6 of the Nucleus for European Modelling of the Ocean (NEMO) framework (Madec et al., 2023). The model uses a high-resolution curvilinear grid configuration at a horizontal resolution of 1/12°, corresponding to approximately 4 to 8.5 km depending on the location. The vertical structure is resolved with 75 z-levels, with finer resolution (1 m) in the upper layers to capture surface processes, decreasing to over 400 m in the deep ocean. The domain spans the northeastern Atlantic Ocean, the North Sea, and the western Mediterranean Sea, covering latitudes 25–65° N and longitudes 21° W–14° E. This geographical extent includes diverse oceanographic features such as wide continental shelves (e.g., the North Sea and English Channel), narrow shelves (e.g., along the Iberian Peninsula), and highly dynamic regions like the Strait of Gibraltar (Maraldi et al., 2013; Sotillo et al., 2015) (Figure 16).

This project has received funding from the European Union's Horizon 2020 research and innovation programme under grant agreement No. 101003598

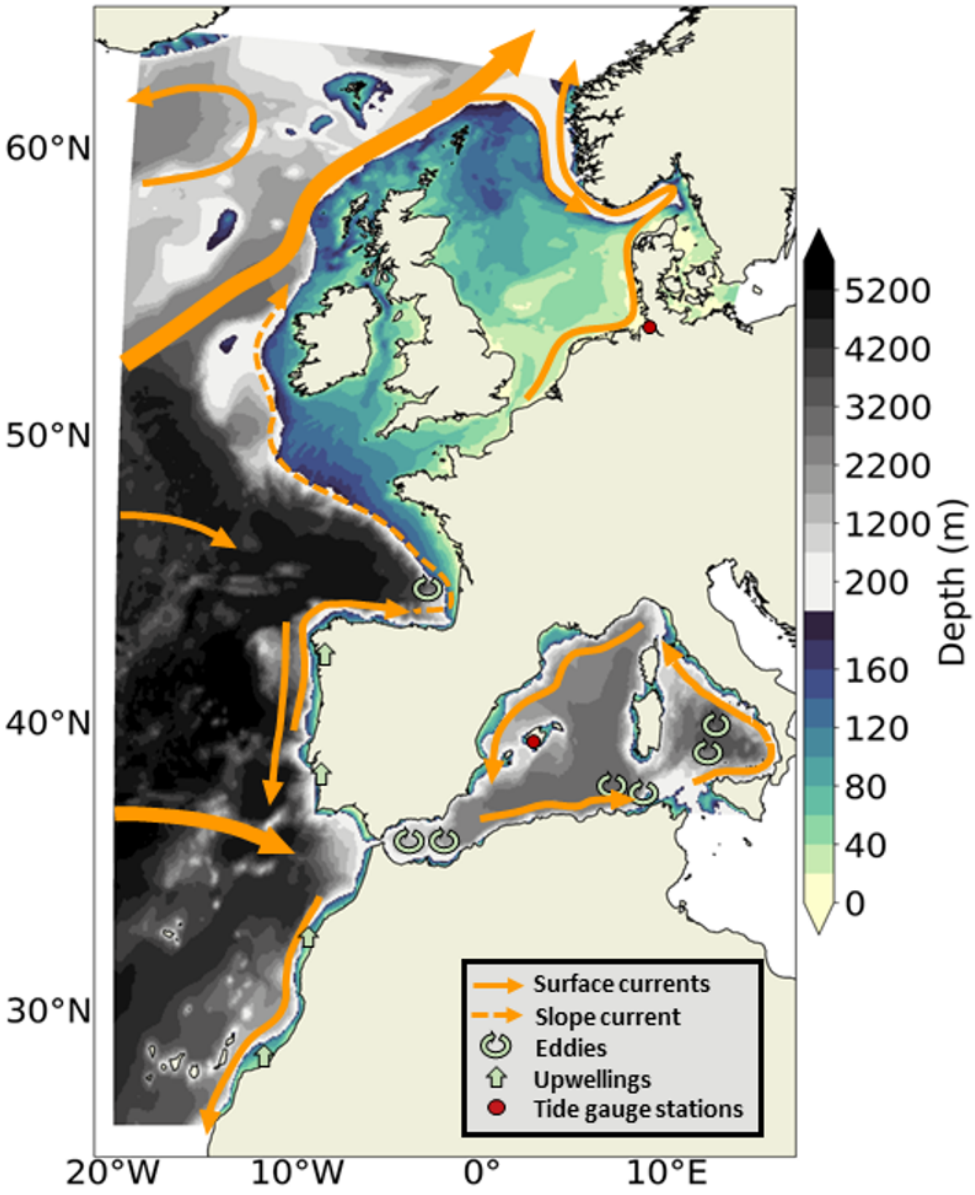

Figure 16. Bathymetry (m) and schematic description of main oceanographic features in the IBI domain. Note that the colour scale for the bathymetry is not linear. The shelf break (defined by the 200 m isobath) is indicated by the change in the colour map).

The IBI-CCS configuration was adapted to improve the resolution and representation of coastal processes compared to its parent model, the CNRM-CM6-1-HR global climate model (Voldoire et al., 2019). CNRM-CM6-1-HR is a coupled model participating in CMIP6 and includes an ocean component with a horizontal resolution of 1/4° (12–25 km at mid-latitudes) and an atmospheric resolution of 1/2° (24–50 km).

This project has received funding from the European Union's Horizon 2020 research and innovation programme under grant agreement No. 101003598

While the GCM provides broad-scale forcing data, its resolution is insufficient to capture finer coastal dynamics such as tides, mesoscale eddies, and atmospheric pressure-induced surges (Fox-Kemper et al., 2021). In contrast, the IBI-CCS model resolves these processes explicitly, thereby enhancing the accuracy and reliability of regional sea level (SL) projections.
The ocean dynamics in IBI-CCS are governed by the hydrostatic and Boussinesq approximations, and the model employs partial step bottom cells to improve bathymetric representation (Barnier et al., 2006). The seawater equation of state is approximated using the TEOS-10 standard in the parent GCM and EOS-80 in the regional model. These differences required consistent conversions of salinity and temperature fields between the models. One of the critical challenges in regional modeling is the propagation of biases and drifts from the parent GCM into the regional model. Climate drifts, caused by insufficient spin-up time in GCMs, can result in long-term unphysical trends in variables like temperature and salinity. In this study, a drift correction was applied to the GCM outputs before using them as boundary and initial conditions for IBI-CCS. The drift correction method involved estimating linear trends from the preindustrial control simulation of CNRM-CM6-1-HR and removing these trends from historical and future simulations. This approach aligns with best practices outlined by Irving et al. (2021) and Fox-Kemper et al. (2021), ensuring that simulated long-term trends reflect external climate forcings rather than model artifacts.
Bias corrections were implemented to address discrepancies between GCM outputs and reference datasets. For oceanic variables, corrections were derived from the GLORYS2V4 ocean reanalysis (Garric et al., 2017), while atmospheric fields were corrected using ERA-Interim reanalysis (Berrisford et al., 2009). Seasonal mean biases were computed over the period 1993–2014 and applied uniformly to the historical and scenario simulations, based on the assumption of stationarity (Xu et al., 2019). These corrections significantly improved the representation of sea surface height (SSH), temperature, and salinity in the regional domain.
Special adjustments were made for the Mediterranean Sea, where biases in SSH and water mass transport through the Strait of Gibraltar were particularly pronounced. Observations and reanalyses indicate that the net exchange of water between the Mediterranean and Atlantic depends on the SSH gradient across the strait (Soto-Navarro et al., 2010). In IBI-CCS, a corrective value of +0.1 m was added to the eastern boundary of the Mediterranean domain to ensure realistic net transport, as validated against reference datasets (Levier et al., 2020).

In CoCliCo, IBI-CCS was further updated to IBI-CCSv2. The new configuration is based on the Primitive Equation NEMO ocean model, version 4.2 (Nucleus for European Modelling of the Ocean, Madec et al., 2023). It has a curvilinear grid at 1/12° resolution (6-7 km) and 75 vertical z-layers, covering the region from 25 to 65N and 21°W to 16°E, including the North Sea and the western Mediterranean Sea (Figure 16). Compared to IBI-CCS, IBI-CCSv2 has an extended domain eastwards in the Mediterranean Sea up to the Strait of Sicily, therefore including the Tyrrhenian Sea;

This project has received funding from the European Union's Horizon 2020 research and innovation programme under grant agreement No. 101003598

an upgraded version of the numerical ocean model (from NEMOv3.6 to NEMOv4.2, including a change in the advection scheme), an updated bathymetry (based on EMODnet 2020), and updated tidal boundary conditions (FES2014, Lyard et al., 2021). In addition, biases and corresponding climatological mean and seasonal cycle corrections are using the GLORYS12v1 ocean reanalysis (Lellouche et al., 2021) and ERA5 atmospheric reanalysis (Herbasch et al., 2020) as references. Finally, regarding the sea level at open ocean boundaries: in IBI-CCSv2, only the ocean dynamic (zos in CMIP6) and the barystatic sea level (obtained through the de-drifted global volume trend, volo in CMIP6), both at monthly resolutions, are imposed. The addition of the barystatic sea level at the model OBs supports consistency between the ocean fields forced at the open boundaries. It must be noted, however, that barystatic sea-level is not necessarily well modelled directly in the GCMs. Besides tidal forcing through OBs and tidal potential, the atmospheric pressure driven sea-level is introduced at the open boundaries using the inverse barometer approximation. Compared to the previous IBI-CCS, which used a constant reference pressure value (Chaigneau et al., 2022), we implement a time-varying reference atmospheric pressure in IBI-CCSv2, computed as the mean global atmospheric pressure field over the ocean for each GCM and scenario.

3.2. Simulations performed

Four CMIP6 global climate models were downscaled with the IBI-CCSv2 configuration (Table 6), under 3 different climate change scenarios. The list of simulations performed in CoCliCo is provided in Table 7.

The choice of CMIP6 global climate models to be downscaled with IBI-CCSv2 in CoCliCo was based on criteria of high-enough temporal and spatial resolutions and availability of simulations for the control, historical, and selected SSPs experiments. Four CMIP6 climate models were selected: CNRM-CM6-1-HR (Voldoire, 2019), CNRM-CM6-1 (Voldoire et al., 2019), EC-Earth3 (Haarsma et al., 2016) and MPI-ESM1-2-HR (Gutjahr et al., 2019).

Table 6. List and characteristics of CMIP6 GCMs that were downscaled with IBI-CCSv2 for CoCliCo. ECS: Equilibrium Climate Sensitivity from Meehl et al. (2020) (CMIP6 range 3.7±1.1°C), which estimates the global mean surface temperature at equilibrium when doubling pre-industrial atmospheric carbon dioxide concentration levels. PSL: Atmospheric sea-level pressure.

CMIP6 model	Atmospheric resolution		Ocean resolution		ECS (°C)
	Spatial	Temporal	Spatial	Temporal	
CNRM-CM6-1-HR	0.5°	3-hourly except 6-hourly PSL	0.25°	Monthly	4.3

This project has received funding from the European Union's Horizon 2020 research and innovation programme under grant agreement No. 101003598

(Voldoire, 2019)		Daily PSL for SSP2-4.5			
CNRM-CM6-1 (Voldoire et al., 2019)	1.4°	3-hourly except 6-hourly PSL Daily PSL for SSP2-4.5	1°	Monthly	4.8
EC-Earth3 (Haarsma et al., 2016)	0.7°	3-hourly except 6-hourly PSL	1°	Monthly	4.3
MPI-ESM1-2-HR (Gutjahr et al., 2019)	0.9°	3-hourly all	0.4	Monthly	3.0

Boundary conditions for the simulations included monthly-averaged ocean variables (temperature, salinity, currents, and SSH) and atmospheric variables (e.g., wind, temperature, and humidity) from the GCM (Table 1). A Flather boundary condition was applied for SSH to preserve consistency between the GCM and RCM, while river runoff inputs were derived directly from the TRIP river-routing scheme of CNRM-CM6-1-HR (Voldoire et al., 2019).

IBI-CCSv2 simulations span the period 1950–2099, divided into historical and future projection phases. The historical simulation (1950–2014) was forced with observed greenhouse gas concentrations, while future projections (2015–2100) were based on three contrasting socio-economic pathways: SSP1-2.6, SSP2-4.5 and SSP5-8.5 (O'Neill et al., 2016), following the integrated scenarios of CoCliCo (Table 2).
SSP1-2.6 represents a low-emission scenario aligned with the Paris Agreement's goal of limiting global warming to below 2°C. This pathway assumes widespread adoption of renewable energy and sustainable practices (Lee et al., 2021). In contrast, SSP5-8.5 describes a high-emission scenario characterized by rapid economic growth driven by fossil fuel use, resulting in significant radiative forcing (approximately 8.5 W/m²) by the end of the century. SSP2-4.5 represents the middle scenario that is most representative of current trends and political commitments towards climate change mitigation, leading to an end of century Earth radiative forcing of 4.5 W/m^2.

In addition, to climate simulations downscaling CMIP6 models, a hindcast was performed over the period 1993-2019. For this hindcast, IBI-CCSv2 is initialized and forced at its lateral ocean boundaries by the GLORYS12v1 ocean reanalysis (Lellouche et al., 2021), while atmospheric forcings are provided by the ERA5 reanalysis (Herbasch et al., 2020). The hindcast provides a reference run over the past decades, using state-of-the-art forcings (also used as a reference for correcting

This project has received funding from the European Union's Horizon 2020 research and innovation programme under grant agreement No. 101003598

biases in CMIP6 forcings, section 3.1), against which we can compare historical simulations forced by CMIP6 models (Table 2) in the following section.

Table 7. List of simulations performed with IBI-CCSv2 in CoCliCo, with corresponding forcing datasets.

Simulation	No. members	Period	Atmospheric forcing	Lateral ocean forcing + initial conditions	River forcing
Hindcast	1	1993-2019	ERA5 (hourly)	GLORYS12V1 (daily)	Climatology (Dai at al. 2017-daily)
Historical	4	1950-2014	corrected GCMs	corrected GCMs	Pre-processed GCMs
SSP1-2.6	4	2015-2099	corrected GCMs	corrected GCMs	Pre-processed GCMs
SSP2-4.5	4	2015-2099	corrected GCMs	corrected GCMs	Pre-processed GCMs
SSP5-8.5	4	2015-2099	corrected GCMs	corrected GCM	Pre-processed GCM

3.3. Validation of Historical Simulations

The initial IBI-CCS model was validated against observational datasets, including the IBIRYS reanalysis and IBI-ERAi simulation, over the historical period 1993–2014. These comparisons demonstrated that the regional model significantly reduced biases relative to the parent GCM (CNRM-CM6-1-HR), particularly in key ocean variables such as sea surface temperature (SST), salinity, and SL. For example, thermosteric and halosteric SL biases present in the GCM were substantially corrected in IBI-CCS due to bias adjustments and the improved resolution of regional processes. The corrections led to a more realistic representation of SL components, with thermosteric contributions aligning closely with IBIRYS and IBI-ERAi (Adloff et al., 2018; Levier et al., 2020).

Special attention was given to the Mediterranean Outflow Water (MOW), a critical water mass influencing regional salinity and SL. In the GCM, large biases in Mediterranean salinity propagated into the Atlantic, altering the characteristics of the MOW (Figure 17, black curve). When the GCM is downscaled without bias correcting the forcings, the same biases are found (Figure 17, grey curve). However, when forcings are corrected, the IBI-CCS downscaling (Figure 17, red curve) leads to a representation of water masses that is much closer to reference datasets (a reanalysis, IBIRYS, yellow curve, and a hindcast, blue curve in Figure 17), leading to

This project has received funding from the European Union's Horizon 2020 research and innovation programme under grant agreement No. 101003598

an improved representation of the MOW's thermohaline properties at approximately 950 m depth (Soto-Navarro et al., 2010). This showcases the importance of bias corrections of CMIP forcings for the high-resolution regional ocean climate simulations.

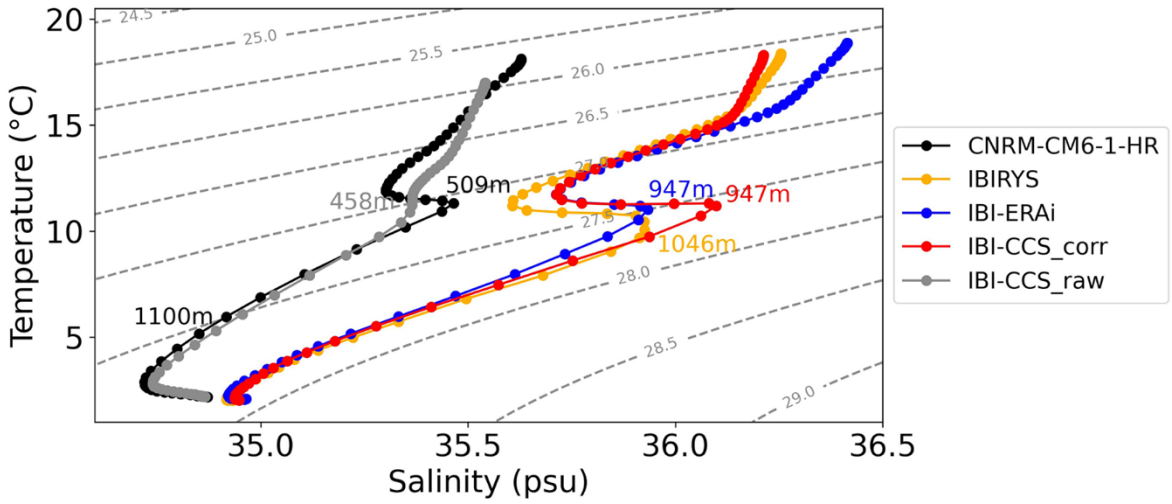

Figure 17. Temperature-Salinity diagram performed westward of Gibraltar Strait to illustrate the water mass properties over the period 1993-2014 for the CMIP6 global climate model CNRM-CM6-1-HR (black), the regional IBI-CCS model downscaling CNRM-CM6-1-HR with no bias corrections (grey), the regional IBI-CCS model downscaling CNRM-CM6-1-HR with bias corrections of forcings (red), and references datasets: the IBIRYS reanalysis, constrained by observations (yellow) and the IBI-CCS-ERAi hindcast forced by reanalyzes (section 3.1, blue).

A more detailed validation of IBI-CCS is provided in Chaigneau et al. (2022).

Based on the preliminary work of Chaigneau et al. (2022), a similar methodology was used in CoCliCo with IBI-CCSv2, with a correction of forcing biases for the mean state and seasonal cycle (Section 3.1).
Since the regional patterns of mean sea level changes mostly depend on ocean circulation (except at high-latitudes where Earth's gravity-rotation-deformation effects associated to mass loss from icesheets and glaciers induce large-scale spatial gradients of sea level), and given that IBI-CCSv2 (as a Primitive Equation ocean general circulation model) can only explicitly represent patterns of ocean dynamic sea level, we focus on this contribution for the comparison of IBI-CCSv2 to global climate models and reference datasets.
The mean sea level patterns induced by ocean circulations is referred to as mean dynamic topography (MDT). The comparison of the MDT in the four CMIP6 global climate models (GCM, Table 1) multi-model ensemble mean (MMM) to the MDT of the IBI-CCSv2 regional MMM is provided in Figure 18(c, d), together with the MDT in two

This project has received funding from the European Union's Horizon 2020 research and innovation programme under grant agreement No. 101003598

reference datasets: the MDT as observed by satellite altimetry (Fig 18a) and the MDT in the IBI-CCSv2 hindcast (Table 2, Fig 18b).

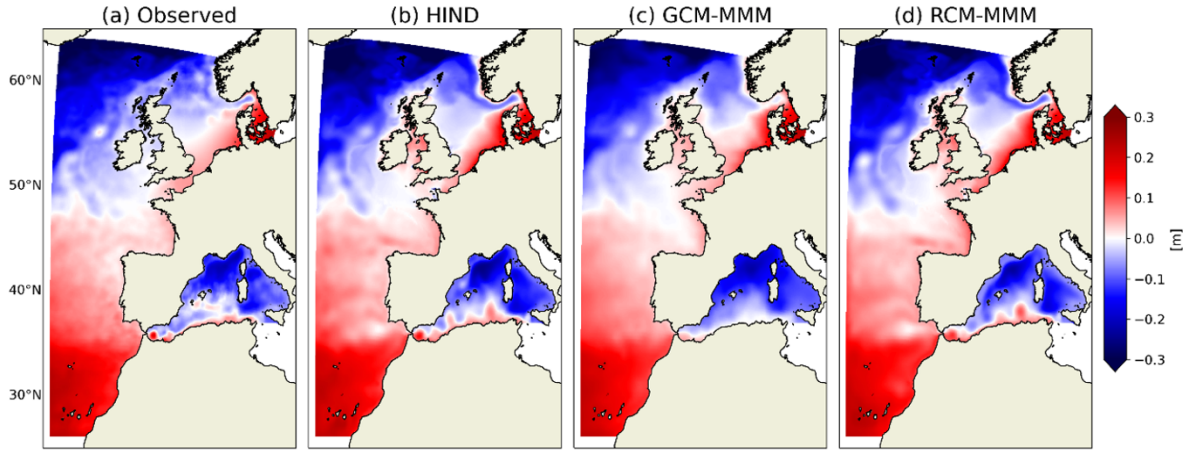

Figure 18. Comparison of mean dynamic topography fields against altimetry observations (MDT-CNES-CLS22 product from AVISO) (a) over 1993-2012. Modelled mean dynamic topography in (b) IBI-CCSv2 hindcast (forced by GLORYS12v1 and ERA5), (c) the four CMIP6 global climate models multi-model ensemble mean, (d), the four IBI-CCSv2 downscaled, regional multi-model mean (MMM). GCM stands for global climate models, RCM stands for regional climate model.

Overall, the modelled MDT (Fig 18b-d) are in good agreement with the observed MDT (Fig 18a). The meridional gradient on the Atlantic Ocean, North Sea and Mediterranean Sea are captured in all modeled results, while models show larger MDT values than observations in the southern North Sea and Irish Sea and along the French Atlantic coast. In general, higher spatial variability is observed in the downscaled simulations (Fig 18b, d) compared to CMIP6 parent models (Fig 18c), including more pronounced mesoscale features. The MDT over the Norwegian Current, the Mediterranean shelf, the Alboran gyre and the Algerian current and resulting eddies are better represented in IBI-CCSv2 results (hindcast, historical climate runs, Fig 18b, d) than in the CMIP6 global climate models (Fig 18c).

In terms of ocean surface circulation, IBI-CCSv2 historical multi-model ensemble mean accurately represents surface circulation patterns (Fig 19c) of the IBI-CCSv2 hindcast (Fig 19a), including the North Atlantic Current, the Iberian Poleward Current, and the Azores Current. These features, poorly resolved in the GCM (Fig 19b), were well reproduced in the regional model, highlighting the added value of dynamical downscaling (Maraldi et al., 2013). These validation results are consistent with these of Chaigneau et al. (2022), with a larger ensemble of downscaled CMIP6 models.

This project has received funding from the European Union's Horizon 2020 research and innovation programme under grant agreement No. 101003598

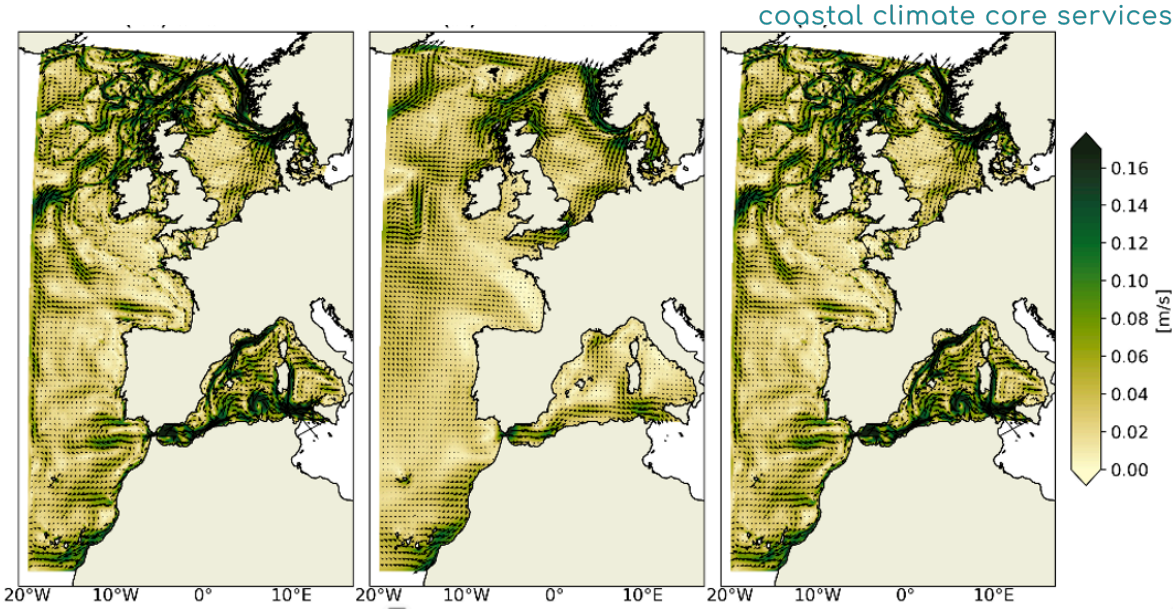

Figure 19. Comparison of the surface mean ocean circulation (in m/s) over 1993-2014 in (left) the IBI-CCSv2 hindcast, (middle) the CMIP6 global climate models multi-model ensemble mean and (left) the IBI-CCSv2 downscaled, regional multi-model ensemble mean (MMM).

3.4. 21st-Century Projections

Results from the future projections (2015–2100) under SSP1-2.6 and SSP5-8.5 scenarios performed with IBI-CCS are documented for mean sea level changes in Chaigneau et al. (2022). The IBI-domain averaged mean SL changes (in m) for the historical period (1970–2014), SSP5-8.5 (solid line) and SSP1-2.6 (dashed line) scenarios (referenced to1986–2005) for the CNRM-CM6-1-HR CMIP6 model and the two regionally downscaled IBI- CCS_raw and IBI-CCS_corr simulations are shown in Figure 20.

By the end of the century, a mean sea level increase of + 80 cm is simulated over the IBI domain for the SSP5-8.5 scenario (relative to 1986–2005) and + 40 cm for the SSP1-2.6 scenario in IBI-CCS (Figure 20, with the global mean thermosteric sea level being accounted for). These values are close to the GMSL projections of + 71 cm (RCP8.5) and + 39 cm (RCP2.6) from Oppenheimer et al. (2019) over the same period. In addition, the consistency of the trend of total regional mean SL between the global and regional simulations for the two scenarios validates the dynamical downscaling technique employed. It demonstrates that bias corrections do not impact the projected mean SL trend for both scenarios that we want to impose in the regional model.

The IBI-CCS model provided higher-resolution insights into SL dynamics compared to the parent GCM. Although the large-scale trends in SL rise were similar between the GCM and RCM, the finer resolution of IBI-CCS allowed for the identification of localized variations, particularly in coastal and shelf regions.

This project has received funding from the European Union's Horizon 2020 research and innovation programme under grant agreement No. 101003598

Thermosteric and halosteric contributions to SL rise varied significantly between the scenarios. Under SSP5-8.5, the thermosteric component dominated, reflecting enhanced ocean warming. In contrast, SSP1-2.6 projections showed a more balanced contribution from halosteric changes, consistent with reduced global warming. The improved representation of salinity gradients in IBI-CCS, achieved through bias corrections, further refined these projections (Church et al., 2013; Meyssignac et al., 2017).

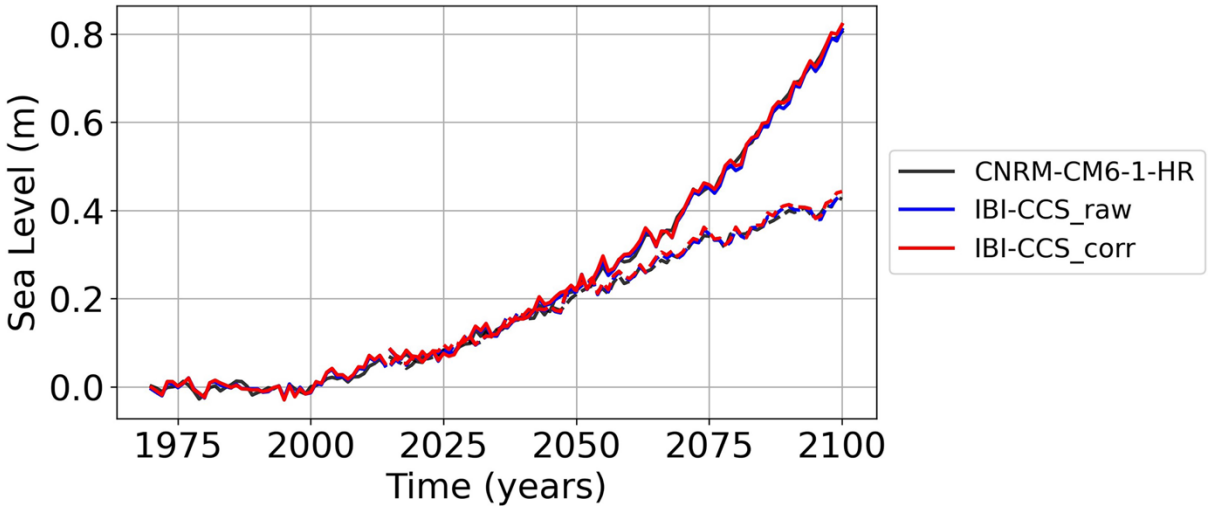

Figure 20. Time series of annual mean SL changes (in m) averaged over the IBI domain for the historical period (1970–2014), SSP5-8.5 (solid line) and SSP1-2.6 (dashed line) scenarios (referenced to1986–2005) for the GCM and the two regionally downscaled IBI-CCS_raw and IBI-CCS_corr simulations.

End of 21st century projected changes in mean ocean dynamic sea level (*mDSL*) over the IBI region and under the SSP5-8.5 scenario are shown in Figure 21 for each of the four CMIP6 climate models downscaled in CoCliCo with IBI-CCSv2 (Table 2). As we focus here on ocean dynamic sea level and since the regional ocean model is based on a Boussinesq model, the domain-mean value is imposed to zero.

The four CMIP6 GCM models exhibit several consistent large-scale projected changes, such as a meridional band of projected increased *mDSL* in the open deep Atlantic, extending to the North Sea and with an intensification along the Norwegian current and Skagerrak/Kattegat. A robust decrease in projected *mDSL* is projected across models in the Mediterranean Sea and along the Atlantic facade. The robustness across models of the projected changes is further illustrated in Figure 22, which shows the GCM MMM projected changes in mean ocean dynamic sea level (*mDSL*) over the IBI region between 1995-2014 and 2080-2099 for the 3 climate change scenarios (SSP1-2.6, SSP2-4.5 and SSP5-8.5). In most of the domain,

This project has received funding from the European Union's Horizon 2020 research and innovation programme under grant agreement No. 101003598

models (at least 3 out of the 4) agree on the sign of changes for all 3 scenarios (see non-hatched regions). Moreover, Figure 22 shows that the projected changes pattern of *mDSL* tend to scale with emission scenarios (the amplitude of projected changes increases as the radiative forcing increases from SSP1-2.6 to SSP2-4.5 and to SSP5-8.5). This builts confidence in an anthropogenically-forced projected change pattern.

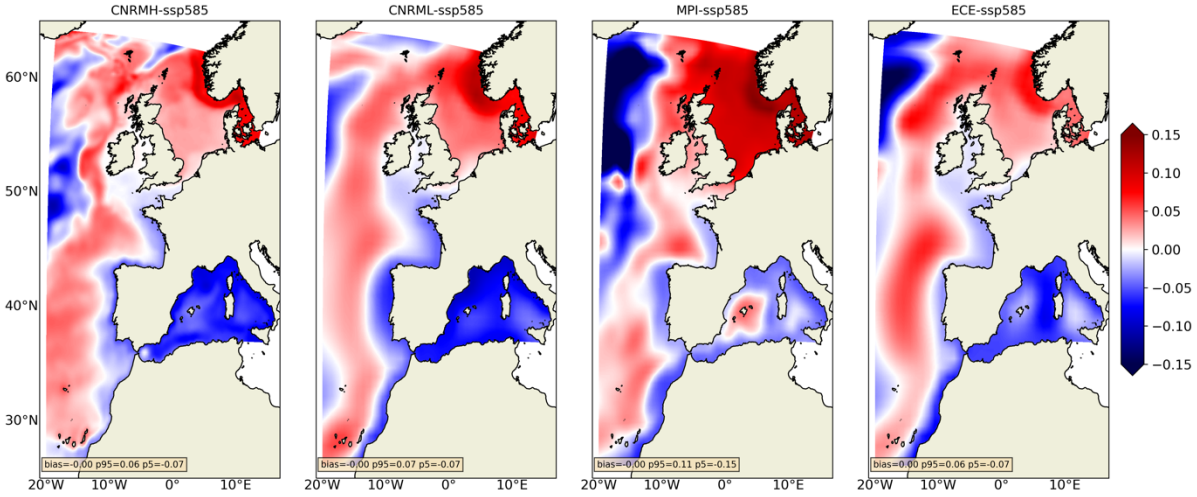

Figure 21. Projected mean ocean dynamic sea level (*mDSL*) changes (in meters) relative to the IBI-domain mean between 1995-2014 and 2080-2099 for SSP5-8.5 for the 4 CMIP6 models (GCM) that are downscaled in CoCliCo with IBI-CCSv2 (Tables 1, 2): (a) CNRM-CM6-1-HR, (b) CNRM-CM6-1, (c) MPI-ESM1-2-HR, (d) EC-Earth3.

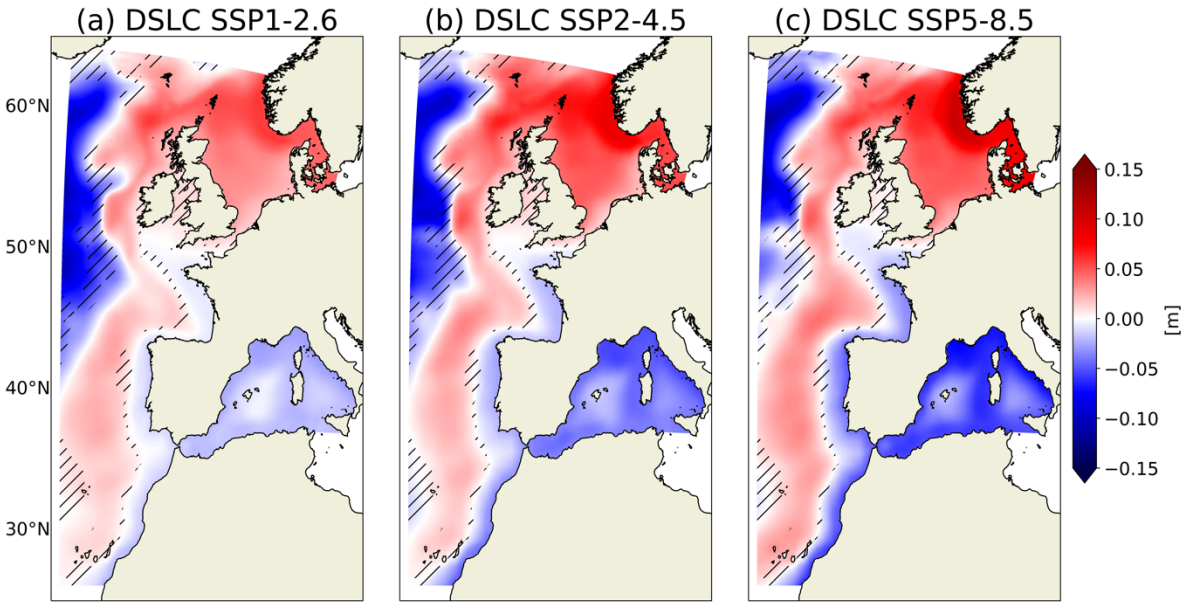

Figure 22. GCM multi-model ensemble mean (MMM) projected changes in mDSL (in meters) between 2080-2099 and 1995-2014 for increasing emission scenarios (a) SSP1.2-6, (b) SSP2-4.5, (c) SSP5-

This project has received funding from the European Union's Horizon 2020 research and innovation programme under grant agreement No. 101003598

8.5. Hatches indicate regions where less than 75% of the models (3/4) agree in sign of the projected change. Panel (c) corresponds to the ensemble mean of Figure 21.

The corresponding end of 21st century IBI-CCSv2 dynamically downscaled projected changes in *mDSL* over the IBI region (relative to the domain-average) and under the SSP5-8.5 scenario are shown in Figure 23 for each of the child simulation.
The high-resolution IBI-CCSv2 projections exhibit several patterns that are consistent between the child (Figure 23) and parent (Figure 21) models.

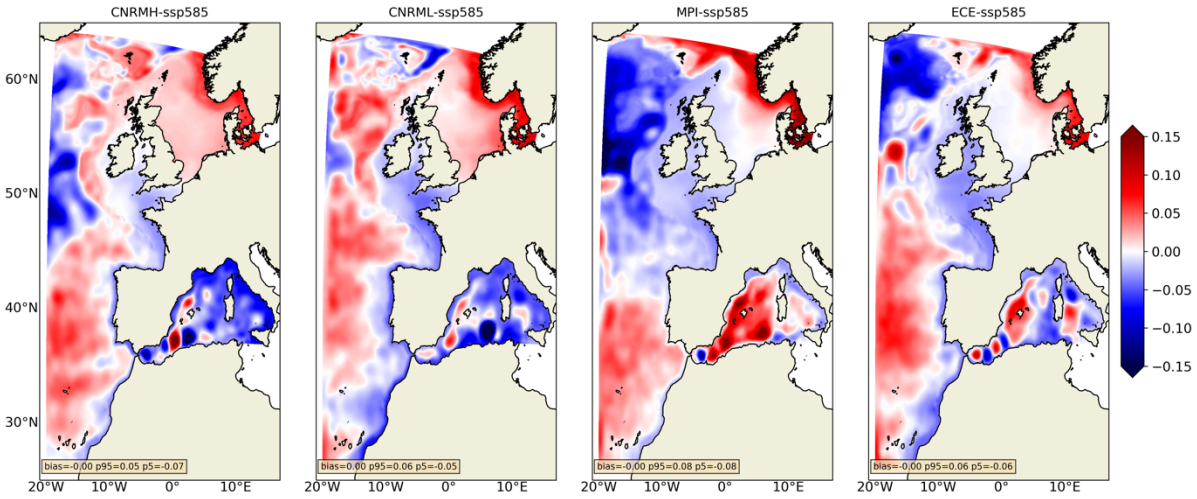

Figure 23. Projected mean ocean dynamic sea level (*mDSL*) changes (in meters) relative to the IBI-domain mean between 1995-2014 and 2080-2099 for SSP5-8.5 for the IBI-CCSv2 dynamical downscaling of the 4 CMIP6 models (Tables 1, 2): (a) CNRM-CM6-1-HR, (b) CNRM-CM6-1, (c) MPI-ESM1-2-HR, (d) EC-Earth3.

As for the global CMIP6 models, the IBI-CCSv2 high-resolution projections agree over most of the IBI region on the sign of changes for all 3 scenarios (see non-hatched regions, Figure 24). Moreover, Figure 24 shows that the high-resolution projected changes pattern of *mDSL* tend to scale with emission scenarios (the amplitude of projected changes increases as the radiative forcing increases from SSP1-2.6 to SSP2-4.5 and to SSP5-8.5).

The high-resolution, regionally downscaled IBI-CCSv2 projections of mDSL are sharing robust features with to the low-resolution CMIP6 models, building confidence in the CMIP6 projections (compare Figures 22 and 24). However, substantial differences are also observed. Compared to the GCM MMM, the high-resolution RCM MMM exhibits a strong decrease of the positive *mDSL* change signal throughout the North Sea and northern UK/Ireland coasts. On the other hand, it exhibits an increase

This project has received funding from the European Union's Horizon 2020 research and innovation programme under grant agreement No. 101003598

in projected *mDSL* along the Atlantic French, Iberian and African façade, as well as for the Mediterranean Sea, with a pronounced amplification signal emerging around the Balearic Islands. These downscaling effects are consistent throughout ensemble members (Figure 23).

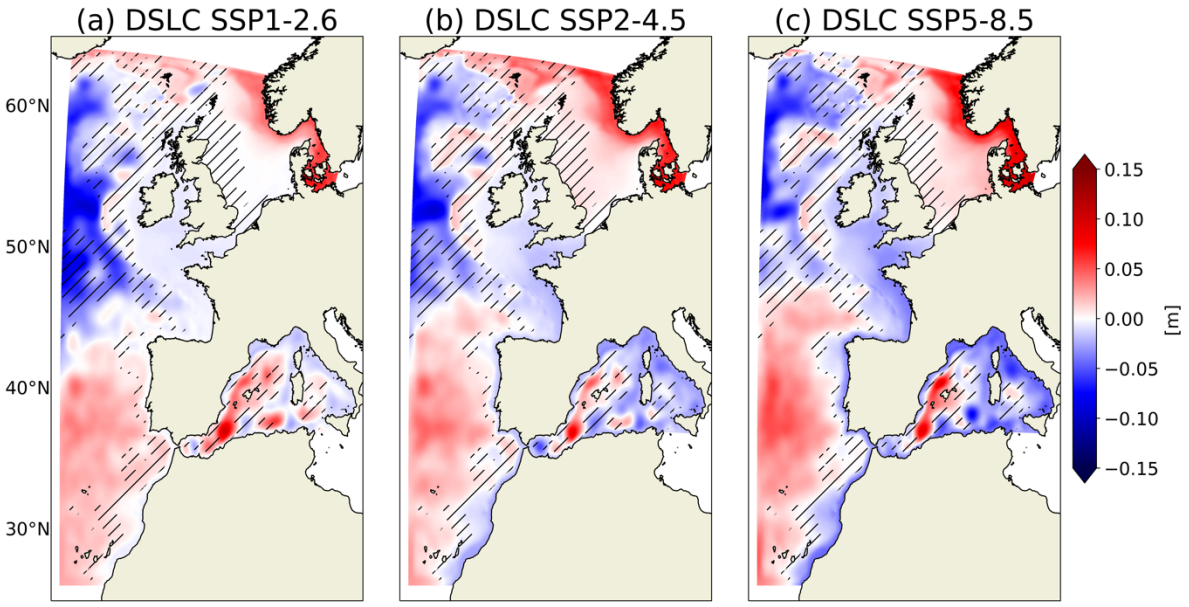

Figure 24. IBI-CCSv2 RCM multi-model ensemble mean (MMM) projected changes in mDSL (in meters) between 2080-2099 and 1995-2014 for increasing emission scenarios (a) SSP1.2-6, (b) SSP2-4.5, (c) SSP5-8.5. Hatches indicate regions where less than 75% of the models (3/4) agree in sign of the projected change. Panel (c) corresponds to the ensemble mean of Figure 23.

Results from the IBI-CCSv2 climate simulations will be submitted in a peer-reviewed international journal in 2025.

In addition, the IBI-CCS regional model was used to assess the impact of dynamically simulating future changes in extreme sea level drivers compared to a static approach that does not consider the impact of climate change on extreme sea level distribution (Chaigneau et al., 2024). This preliminary study (downscaling only 1 CMIP6 model, CNRM-CM6-1-HR, section 3.1) showcased that the impact of simulating dynamic changes in extremes was statistically significant in the Mediterranean Sea, with differences in the decennial return level of up to +20 % compared to the static approach. Chaigneau et al. (2024) attributed this result to the refined mean sea level rise simulated by the regional ocean general circulation model. In CoCliCo, although the high-resolution sea level projections are targeting mean sea level changes for the present deliverable, the question of projected changes in extreme sea levels could also be addressed with the simulations produced with IBI-CCSv2.

This project has received funding from the European Union's Horizon 2020 research and innovation programme under grant agreement No. 101003598

4. References

Adloff, F., Jordà, G., Somot, S., Sevault, F., Arsouze, T., Dubois, C., Padorno, E., Alvarez-Fanjul, E., and Gomis, D.: Improving Sea level simulation in Mediterranean regional climate models, Clim. Dynam., 51, 1167–1178, https://doi.org/10.1007/s00382-017-3842-3, 2018.

Adloff, F., Somot, S., Sevault, F., Jorda, G., Aznar, R., Déqué, M., Herrmann, M., Marcos, M., Dubois, C., and Padorno, E.: Impact of climate change on the Western Mediterranean Sea: Results from a regional ocean circulation model, Clim. Dynam., 45, 1097–1119, https://doi.org/10.1007/s00382-015-2507-3.

Allen MR, Smith LA (1997) Optimal filtering in singular spectrum analysis. Phys Lett A 234(6):419–428.

Anav A, Friedlingstein P, Kidston M, Bopp L, Ciais P, Cox P, Jones C, Jung M, Myneni R, Zhu Z (2013) Evaluating the land and ocean components of the global carbon cycle in the CMIP5 earth system models. J Clim 26(18):6801–6843.

Anav A, Carillo A, Palma M, Struglia MV, Turuncoglu UU, Sannino G (2021) The ENEA-REG system (v1.0), a multi-component regional Earth system model: sensitivity to different atmospheric components over the Med-CORDEX (coordinated regional climate downscaling experiment) region. Geosci Model Dev 14(7):4159–4185.

Artale V, Calmanti S, Carillo A, Dell'Aquila A, Herrmann M, Pisacane G, Ruti PM, Sannino G, Struglia MV, Giorgi F (2010) An atmosphere–ocean regional climate model for the Mediterranean area: assessment of a present climate simulation. Clim Dyn 35:721–740.

Baladrón, C., Sotillo, M. G., Aznar, R., Levier, B., Amo-Baladron, A., Paramo, J., and Sánchez-Román, A.: IBI ocean reanalysis: A multi-decadal, high-resolution dataset for the Iberian-Biscay-Ireland region, Earth Syst. Sci. Data, 12, 2767–2790, https://doi.org/10.48670/moi-00029.

Barnier, B., Madec, G., Penduff, T., Molines, J.-M., Treguier, A.-M., Le Sommer, J., Beckmann, A., Biastoch, A., Böning, C., Dengg, J., Derval, C., Durand, E., Gulev, S., Remy, E., Talandier, C., Theetten, S., Maltrud, M., McClean, J., and De Cuevas, B.: Impact of partial steps and momentum advection schemes in a global ocean circulation model at eddy-permitting resolution, Ocean Dynam., 56, 543–567, https://doi.org/10.1007/s10236-006-0082-1, 2006.

Berrisford, P., Dee, D., Fielding, K., Fuentes, M., Kallberg, P., Kobayashi, S., and Uppala, S.: The ERA-Interim Archive, ERA report series, European Centre for Medium-Range Weather Forecasts, Shinfield Park, Reading, 16 pp., https://www.ecmwf.int/node/8173 (last access: 7 March 2022), 2009.

Bruyère CL, Done JM, Holland GJ, Fredrick S (2014) Bias corrections of global models for regional climate simulations of high-impact weather. Clim Dyn 43:1847–1856.

This project has received funding from the European Union's Horizon 2020 research and innovation programme under grant agreement No. 101003598

Campin J-M, Adcroft A, Hill C, Marshall J (2004) Conservation of properties in a free-surface model. Ocean Model 6(3–4):221–244.

Cardoso RM, Soares PM (2022) Is there added value in the EURO-CORDEX hindcast temperature simulations? Assessing the added value using climate distributions in Europe. Int J Climatol 42(7):4024–4039.

Chaigneau, A. A., Reffray, G., Voldoire, A., and Melet, A.: IBI-CCS: a regional high-resolution model to simulate sea level in western Europe, Geosci. Model Dev., 15, 2035–2062, https://doi.org/10.5194/gmd-15-2035-2022, 2022.

Chaigneau, A. A., Melet, A., Voldoire, A., Irazoqui Apecechea, M., Reffray, G., Law-Chune, S., and Aouf, L.: Dynamic projections of extreme sea levels for western Europe based on ocean and wind-wave modelling, Nat. Hazards Earth Syst. Sci., 24, 4031–4048, https://doi.org/10.5194/nhess-24-4031-2024, 2024.

Chen, X., et al.: Emergent constraints on climate sensitivity: A review, Nature, 563, 547–550, https://doi.org/10.1038/s41586-019-1751-x, 2020.

Christensen JH, Christensen OB (2007) A summary of the PRUDENCE model projections of changes in European climate by the end of this century. Clim Change 81:7–30.

Church, J. A., Clark, P. U., et al.: Sea level change, in: Climate Change 2013: The Physical Science Basis, Cambridge University Press, Cambridge, UK, and New York, NY, USA, https://doi.org/10.1017/CBO9781107415324.026, 2013.

Ciais P, Reichstein M, Viovy N, Granier A, Ogée J, Allard V, Aubinet M, Buchmann N, Bernhofer C, Carrara A (2005) Europe-wide reduction in primary productivity caused by the heat and drought in 2003. Nature 437(7058):529–533.

Cos J, Doblas-Reyes F, Jury M, Marcos R, Bretonnière P-A, Samsó M (2022) The Mediterranean climate-change hotspot in the CMIP5 and CMIP6 projections. Earth Syst Dynam 13:321–340.

Darmaraki S, Somot S, Sevault F, Nabat P, Cabos Narvaez WD, Cavicchia L, Djurdjevic V, Li L, Sannino G, Sein DV (2019) Future evolution of marine heatwaves in the Mediterranean Sea. Clim Dyn 53:1371–1392.

Dubois C, Somot S, Calmanti S, Carillo A, Déqué M, Dell'Aquila A, Elizalde A, Gualdi S, Jacob D, L'Hévéder B, Li L, Oddo P, Sannino G, Scoccimarro E, Sevault F (2012) Future projections of the surface heat and water budgets of the Mediterranean Sea in an ensemble of coupled atmosphere-ocean regional climate models. Clim Dyn 39:1859–1884.

EMODnet Bathymetry Consortium. (2020). EMODnet Digital Bathymetry (DTM 2020) [Dataset]. EMODnet Bathymetry Consortium. https://doi.org/10.12770/BB6A87DD-E579-4036-ABE1-E649CEA9881A

Eyring V, Bony S, Meehl GA, Senior CA, Stevens B, Stouffer RJ, Taylor KE (2016) Overview of the coupled model intercomparison project phase 6 (CMIP6) experimental design and organization. Geosci Model Dev 9(5):1937–1958.

This project has received funding from the European Union's Horizon 2020 research and innovation programme under grant agreement No. 101003598

Fantini A, Raffaele F, Torma C, Bacer S, Coppola E, Giorgi F, Ahrens B, Dubois C, Sanchez E, Verdecchia M (2018) Assessment of multiple daily precipitation statistics in ERA-Interim driven Med-CORDEX and EURO-CORDEX experiments against high-resolution observations. Clim Dyn 51:877–900.

Fox-Kemper B, Menemenlis D (2008) Can large eddy simulation techniques improve mesoscale rich ocean models? Washington DC Am Geophys Union Geophys Monogr Ser 177:319–337.

Fox-Kemper, B., Hewitt, H. T., Xiao, C., Aðalgeirsdóttir, G., Drijfhout, S. S., Edwards, T. L., Golledge, N. R., Hemer, M., Kopp, R. E., Krinner, G., Mix, A., Notz, D., Nowicki, S., Nurhati, I. S., Ruiz-Barradas, A., and Schuur, E. A. G.: Ocean, cryosphere, and sea level change, in: Climate Change 2021: The Physical Science Basis, Cambridge University Press, Cambridge, UK, 1211–1362, https://www.ipcc.ch/site/assets/uploads/sites/3/2019/11/SROCC_FOD_Ch03_Final.pdf, 2021.

Garric, G., Parent, L., and Drévillon, M.: Performance assessment of the CMEMS GLORYS2V4 global ocean reanalysis, Ocean Sci., 13, 281–302, https://doi.org/10.5194/os-13-281-2017, 2017.

Giorgi F, Gutowski WJ Jr (2015) Regional dynamical downscaling and the CORDEX initiative. Annu Rev Environ Resour 40:467–490.

Gregory, J. M., Griffies, S. M., Hughes, C. W., Lowe, J. A., Church, J. A., Fukimori, I., Gomez, N., Kopp, R. E., Landerer, F., Cozannet, G. L., Ponte, R. M., Stammer, D., Tamisiea, M. E., and van de Wal, R. S. W.: Concepts and Terminology for Sea Level: Mean, Variability and Change, Both Local and Global, Surveys in Geophysics, 40, 1251–1289, https://doi.org/10.1007/s10712-019-09525-z, 2019.

Gutjahr O, Putrasahan D, Lohmann K, Jungclaus JH, von Storch J-S, Brüggemann N, Haak H, Stössel A (2019) Max planck institute earth system model (MPI-ESM1.2) for the high-resolution model intercomparison project (HighResMIP). Geosci Model Dev 12(7):3241–3281.

Haarsma, R. J., Roberts, M. J., Vidale, P. L., Senior, C. A., Bellucci, A., Bao, Q., Chang, P., Corti, S., Fučkar, N. S., Guemas, V., von Hardenberg, J., Hazeleger, W., Kodama, C., Koenigk, T., Leung, L. R., Lu, J., Luo, J.-J., Mao, J., Mizielinski, M. S., … von Storch, J.-S. (2016). High Resolution Model Intercomparison Project (HighResMIP v1.0) for CMIP6. Geoscientific Model Development, 9(11), 4185–4208. https://doi.org/10.5194/gmd-9-4185-2016

Hagemann S, Dümenil L (1997) A parametrization of the lateral water flow for the global scale. Clim Dyn 14:17–31.

Hersbach, H., Bell, B., Berrisford, P., Hirahara, S., Horányi, A., Muñoz-Sabater, J., Nicolas, J., Peubey, C., Radu, R., Schepers, D., Simmons, A., Soci, C., Abdalla, S., Abellan, X., Balsamo, G., Bechtold, P., Biavati, G., Bidlot, J., Bonavita, M., … Thépaut, J. (2020). The ERA5 global reanalysis. Quarterly Journal of the Royal Meteorological Society, 146(730), 1999–2049. https://doi.org/10.1002/qj.3803

Hermans, T. H. J., Slangen, A. B. A., Adloff, F., Jordà, G., and van de Wal, R. S. W.: Future sea level changes for a high-end emission scenario along the northwestern European shelf based on a high-resolution ocean model, Clim. Dynam., 55, 2757–2777, https://doi.org/10.1007/s00382-020-05446-7, 2020b.

Irving, D., Hobbs, W., Church, J., and Zika, J.: A Mass and Energy Conservation Analysis of Drift in the CMIP6 Ensemble, J. Climate, 34, 3157–3170, https://doi.org/10.1175/JCLI-D-20-0281.1, 2021.

This project has received funding from the European Union's Horizon 2020 research and innovation programme under grant agreement No. 101003598

Jacob D, Petersen J, Eggert B, Alias A, Christensen OB, Bouwer LM, Braun A, Colette A, Déqué M, Georgievski G (2014) EURO-CORDEX: new high-resolution climate change projections for European impact research. Reg Environ Change 14:563–578.

Jiménez, J. A., Winter, G., Bonaduce, A., Depuydt, M., Galluccio, G., van den Hurk, B., Meier, H. E. M., Pinardi, N., Pomarico, L. G., and Vazquez Riveiros, N.: Sea Level Rise in Europe: Knowledge gaps identified through a participatory approach, State of the Planet, 3-slre1, 3, https://doi.org/10.5194/sp-3-slre1-3-2024, 2024.

Kotlarski S, Keuler K, Christensen OB, Colette A, Déqué M, Gobiet A, Goergen K, Jacob D, Lüthi D, Van Meijgaard E (2014) Regional climate modeling on European scales: a joint standard evaluation of the EURO-CORDEX RCM ensemble. Geosci Model Dev 7(4):1297–1333.

Lee, J.-Y., Marotzke, J., Bala, G., Cao, L., Corti, S., Dunne, J. P., Engelbrecht, F., Fischer, E., Fyfe, J. C., Jones, C., Maycock, A., Mutemi, J., Ndiaye, O., Panickal, S., and Zhou, T.: Future Global Climate: Scenario-Based Projections and Near-Term Information, in: Climate Change 2021: The Physical Science Basis, Contribution of Working Group I to the Sixth Assessment Report of the Intergovernmental Panel on Climate Change, edited by: Masson-Delmotte, V., Zhai, P., Pirani, A., Connors, S. L., Péan, C., Berger, S., Caud, N., Chen, Y., Goldfarb, L., Gomis, M. I., Huang, M., Leitzell, K., Lonnoy, E., Matthews, J. B. R., Maycock, T. K., Waterfield, T., Yelekçi, O., Yu, R., and Zhou, B., Cambridge University Press, 2021.

Leith CE (1968) Diffusion approximation for two-dimensional turbulence. Phys Fluids 11:671–673.

Lellouche, J.-M., Greiner, E., Bourdallé-Badie, R., Garric, G., Melet, A., Drévillon, M., Bricaud, C., Hamon, M., Le Galloudec, O., Regnier, C., Candela, T., Testut, C.-E., Gasparin, F., Ruggiero, G., Benkiran, M., Drillet, Y., and Le Traon, P. Y.: The Copernicus Global 1/12° Oceanic and Sea Ice GLORYS12 Reanalysis, Front. Earth Sci., 9, 698876, https://doi.org/10.3389/feart.2021.698876, 2021.

Levier, B., Sotillo, M. G., and Cailleau, S.: The IBI ocean reanalysis from 1993 to 2014: Inter-annual analysis of temperature, salinity and currents, Ocean Sci., 16, 295–319, https://doi.org/10.5194/os-16-295-2020, 2020.

Lyard, F. H., Allain, D. J., Cancet, M., Carrère, L., & Picot, N. (2021). FES2014 global ocean tide atlas: Design and performance. Ocean Science, 17(3), 615–649. https://doi.org/10.5194/os-17-615-2021

Madec, G., Bell, M., Blaker, A., Bricaud, C., Bruciaferri, D., Castrillo, M., Calvert, D., Jérômeme Chanut, Clementi, E., Coward, A., Epicoco, I., Éthé, C., Ganderton, J., Harle, J., Hutchinson, K., Iovino, D., Lea, D., Lovato, T., Martin, M., … Wilson, C. (2023). NEMO Ocean Engine Reference Manual. https://doi.org/10.5281/ZENODO.8167700

Maraldi, C., Chanut, J., Levier, B., Ayoub, N., De Mey, P., Reffray, G., Lyard, F., Cailleau, S., Drévillon, M., Fanjul, E. A., Sotillo, M. G., Marsaleix, P., and the Mercator Research and Development Team: NEMO on the shelf: assessment of the Iberia–Biscay–Ireland configuration, Ocean Sci., 9, 745–771, https://doi.org/10.5194/os-9-745-2013, 2013.

Marshall J, Adcroft A, Hill C, Perelman L, Heisey C (1997) A finite-volume, incompressible Navier Stokes model for studies of the ocean on parallel computers. J Geophys Res Oceans 102(C3):5753–5766.

This project has received funding from the European Union's Horizon 2020 research and innovation programme under grant agreement No. 101003598

McInnes, K. L., Nicholls, R. J., Van De Wal, R., Behar, D., Haigh, I. D., Hamlington, B. D., Hinkel, J., Hirschfeld, D., Horton, B. P., Melet, A., Palmer, M. D., Robel, A. A., Stammer, D., and Sullivan, A.: Perspective on Regional Sea-level Change and Coastal Impacts, Camb. prisms Coast. futures, 2, e16, https://doi.org/10.1017/cft.2024.15, 2024.

Melet, A., Meyssignac, B., Almar, R., and Le Cozannet, G.: Under-estimated wave contribution to coastal sea-level rise, Nat. Clim. Change, 8, 234–239, https://doi.org/10.1038/s41558-018-0087-z, 2018.

Melet, A., van de Wal, R., Amores, A., Arns, A., Chaigneau, A. A., Dinu, I., Haigh, I. D., Hermans, T. H. J., Lionello, P., Marcos, M., Meier, H. E. M., Meyssignac, B., Palmer, M. D., Reese, R., Simpson, M. J. R., and Slangen, A. B. A.: Sea Level Rise in Europe: Observations and projections, State of the Planet, 3-slre1, 4, https://doi.org/10.5194/sp-3-slre1-4-2024, 2024.

Meyssignac, B., Piecuch, C. G., Merchant, C. J., Racault, M.-F., Palanisamy, H., MacIntosh, C., Sathyendranath, S., and Brewin, R.: Causes of the Regional Variability in Observed Sea Level, Sea Surface Temperature and Ocean Colour Over the Period 1993–2011, Surv. Geophys., 38, 187–215, https://doi.org/10.1007/s10712-016-9383-1, 2017.

Mooney P, Mulligan F, Fealy R (2013) Evaluation of the sensitivity of the weather research and forecasting model to parameterization schemes for regional climates of Europe over the period 1990–95. J Clim 26(3):1002–1017.

O'Neill BC, Tebaldi C, Van Vuuren DP, Eyring V, Friedlingstein P, Hurtt G, Knutti R, Kriegler E, Lamarque J-F, Lowe J (2016) The scenario model intercomparison project (ScenarioMIP) for CMIP6. Geosci Model Dev 9(9):3461–3482.

Oppenheimer, M., Glavovic, B., Hinkel, J., van de Wal, R. S. W., Magnan, A., Abd-Elgawad, A., Cai, R., Cifuentes-Jara, M., DeConto, R. M., Ghosh, T., Hay, J., Isla, F. I., Marzeion, B., Meyssignac, B., & Sebesvari, Z. (2019). Sea Level Rise and Implications for Low Lying Islands, Coasts and Communities. In IPCC Special Report on the Ocean and Cryosphere in a Changing Climate (Pörtner H.-O. et al.). Cambridge University Press.

Pinardi N, Masetti E (2000) Variability of the large-scale general circulation of the Mediterranean Sea from observations and modelling: a review. Palaeogeogr Palaeoclimatol Palaeoecol 158(3–4):153–173.

Richon C, Dutay J-C, Bopp L, Le Vu B, Orr JC, Somot S, Dulac F (2019) Biogeochemical response of the Mediterranean Sea to the transient SRES-A2 climate change scenario. Biogeosciences 16(1):135–165.

Ruti PM, Somot S, Giorgi F, Dubois C, Flaounas E, Obermann A, Dell'Aquila A, Pisacane G, Harzallah A, Lombardi E (2016) MED-CORDEX initiative for Mediterranean climate studies. Bull Am Meteor Soc 97(7):1187–1208.

Sannino G, Carillo A, Iacono R, Napolitano E, Palma M, Pisacane G, Struglia M (2022) Modelling present and future climate in the Mediterranean Sea: a focus on sea-level change. Clim Dyn 59(1–2):357–391.

This project has received funding from the European Union's Horizon 2020 research and innovation programme under grant agreement No. 101003598

Somot S, Sevault F, Déqué M, Crépon M (2008) 21st century climate change scenario for the Mediterranean using a coupled atmosphere–ocean regional climate model. Global Planet Change 63(2–3):112–126.

Sotillo, M. G., Cailleau, S., Lorente, P., Levier, B., Aznar, R., Reffray, G., Amo-Baladrón, A., Chanut, J., Benkiran, M., and Alvarez-Fanjul, E.: The MyOcean IBI Ocean Forecast and Reanalysis Systems: operational products and roadmap to the future Copernicus Service, J. Oper. Oceanogr., 8, 63–79, https://doi.org/10.1080/1755876X.2015.1014663, 2015.

Soto-Navarro, J., et al.: Modeling Mediterranean-Atlantic water exchanges, Prog. Oceanogr., 87, 144–157, https://doi.org/10.5194/os-14-1547-2018.

Storto A, Hesham Essa Y, de Toma V, Anav A, Sannino G, Santoleri R, Yang C (2023) MESMAR v1: a new regional coupled climate model for downscaling, predictability, and data assimilation studies in the Mediterranean region. Geosci Model Dev 16(16):4811–4833.

Taranu IS, Somot S, Alias A, Boé J, Delire C (2023) Mechanisms behind large-scale inconsistencies between regional and global climate model-based projections over Europe. Clim Dyn 60(11–12):3813–3838.

Tebaldi C, Debeire K, Eyring V, Fischer E, Fyfe J, Friedlingstein P, Knutti R, Lowe J, O'Neill B, Sanderson B (2020) Climate model projections from the scenario model intercomparison project (ScenarioMIP) of CMIP6. Earth Syst Dyn 12:253–293.

Tuel A, Eltahir EA (2020) Why is the Mediterranean a climate change hot spot? J Clim 33(14):5829–5843.

Voldoire, A., Saint-Martin, D., Sénési, S., Decharme, B., Alias, A., Chevallier, M., Colin, J., Guérémy, J. -F., Michou, M., Moine, M. -P., Nabat, P., Roehrig, R., Salas y Mélia, D., Séférian, R., Valcke, S., Beau, I., Belamari, S., Berthet, S., Cassou, C., … Waldman, R. (2019). Evaluation of CMIP6 DECK Experiments With CNRM-CM6-1. Journal of Advances in Modeling Earth Systems, 11(7), 2177–2213. https://doi.org/10.1029/2019MS001683

Woodworth, P. L., Menéndez, M., and Gehrels, W. R.: Evidence for century timescale acceleration in mean sea levels and for recent changes in extreme sea levels, Surv. Geophys., 40, 1391–1411, https://doi.org/10.1007/s10712-011-9112-8, 2019.

Xu, Z., Han, Y., and Yang, Z.: Dynamical downscaling of regional climate: A review of methods and limitations, Sci. China Earth Sci., 62, 365–375, https://doi.org/10.1007/s11430-018-9261-5, 2019.

Zuo H, Balmaseda MA, Tietsche S, Mogensen K, Mayer M (2019) The ECMWF operational ensemble reanalysis–analysis system for ocean and sea ice: a description of the system and assessment. Ocean Sci 15(3):779–808.

This project has received funding from the European Union's Horizon 2020 research and innovation programme under grant agreement No. 101003598